REPORT DOCUMENTATION PAGE

Form Approved
OMB No. 0704-0188

1. AGENCY USE ONLY (Leave blank)	2. REPORT DATE	3. REPORT TYPE AND DATES COVERED
	6/1/96	Final 1/16/93 - 1/15/96

4. TITLE AND SUBTITLE

The Forced Turbulent Wall Jet Effects of Pressure Gradient and Curvature

5. FUNDING NUMBERS

F49620-93-1-0050

2307/BS

6. AUTHOR(S)

Professor Israel Wygnanski

7. PERFORMING ORGANIZATION NAME(S) AND ADDRESS(ES)

Aerospace and Mechanical Engineering
College of Engineering and Mines
The University of Arizona
Tucson, Arizona 85721

AFOSR-TR-96

0386

9. SPONSORING/MONITORING AGENCY NAME(S) AND ADDRESS(ES)

Air Force Office of Scientific Research (AFOSR)
AFOSR/NA
110 Duncan Avenue, Suite B115
Bolling AFB, DC 20332-0001

NA

10. SPONSORING/MONITORING AGENCY REPORT NUMBER

93-1-0050

11. SUPPLEMENTARY NOTES

12a. DISTRIBUTION/AVAILABILITY STATEMENT

Approved for Public Release
Distribution is Unlimited

12b. DISTRIBUTION CODE

19960726 091

13. ABSTRACT (Maximum 200 words)

The studies completed in the period of the proposal were in three parts: 1. Both hot wire and PIV data have been obtained on the Coanda cylinder. Strong influences of curvature and of the pressure gradient on the mean and the turbulence quantities were found. New structures were observed around the cylinder in the forced case. A theoretical model was established for the mean flow, which will be an important tool in the further stability studies. 2. Two types of weak wall jet have been observed. Length and velocity scales were found and applied in successful normalization of the mean velocity profiles. Furthermore, three instability modes, coupled to each other, were investigated through forcing. 3.A novel technique for identification of coherent motions was developed which can eliminate the influence of phase jitter and discover much more coherent energy than the conventional phase locked ensemble averaging technique, based on which a reasonable coherent energy budget was established for the first time . This technique will be applied to explore the role of coherent motion in the control of separation.

14. SUBJECT TERMS	15. NUMBER OF PAGES	16. PRICE CODE
	39	

17. SECURITY CLASSIFICATION OF REPORT	18. SECURITY CLASSIFICATION OF THIS PAGE	19. SECURITY CLASSIFICATION OF ABSTRACT	20. LIMITATION OF ABSTRACT
Unclassifed	Unclassified	Unclassified	Unlimited

DISCLAIMER NOTICE

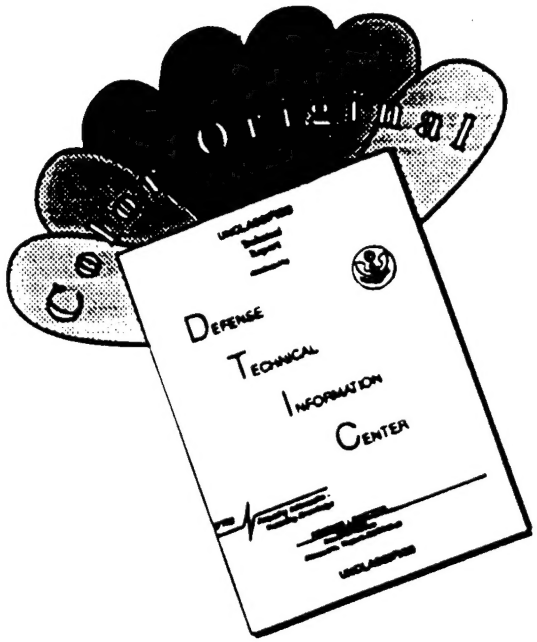

THIS DOCUMENT IS BEST QUALITY AVAILABLE. THE COPY FURNISHED TO DTIC CONTAINED A SIGNIFICANT NUMBER OF COLOR PAGES WHICH DO NOT REPRODUCE LEGIBLY ON BLACK AND WHITE MICROFICHE.

The final report to AFOSR grant No.F49620-93-0050

THE FORCED TURBULENT WALL JET
EFFECTS OF PRESSURE GRADIENT AND CURVATURE

Principal investigator: I. Wygnanski

Department of Aerospace Mechanical Engineering
The University of Arizona

May, 1996

Abstract

The studies completed in the period of the proposal were in three parts: 1. Both hot wire and PIV data have been obtained on the Coanda cylinder. Strong influences of curvature and of the pressure gradient on the mean and the turbulence quantities were found. New structures were observed around the cylinder in the forced case. A theoretical model was established for the mean flow, which will be an important tool in the further stability studies. 2. Two types of weak wall jet have been observed. Length and velocity scales were found and applied in successful normalization of the mean velocity profiles. Furthermore, three instability modes, coupled to each other, were investigated through forcing. 3.A novel technique for identification of coherent motions was developed which can eliminate the influence of phase jitter and discover much more coherent energy than the conventional phase locked ensemble averaging technique, based on which a reasonable coherent energy budget was established for the first time . This technique will be applied to explore the role of coherent motion in the control of separation.

INTRODUCTION

The experiments conducted in Tel Aviv (Seifert, A et al. 1993) showed success in applying oscillatory blowing on a generic flap to obtain high lift. The experiment in Chicargo (unpublished) showed further that this technique is also applicable to compressible flow and has a bright future for applications. The physical mechanism is, however, not yet clear and systematic research on the influence of the governing parameters has not yet been done.

The flow over the generic flap is complex (Fig.1). The mean velocity profile at x/c=0.8 is a thin, weak wall jet embedded in a thick upstream boundary layer on a curved surface. Understanding of the instability of a wall jet with curvature in an external stream and of the structures in the weak wall jet are keys to understanding the dominant mechanisms in this flow and to the achievement of high lift. The downstream region is a separated-reattached flow on a surface at fairly high angle of attack. The unforced profiles at x/c=0.80 - 0.98 (Fig.1) are typical of separated flows. A photo taken in the same region under forcing (Fig.2) shows clearly that the

flow was reattached with traveling vortices embedded in a curved external potential flow field on the upper surface of the flap. In order to understand the entire mechanism and also to determine and to optimize the control parameters, detailed studies of all of these flows are necessary, including a more profound study into the identification of coherent motions in the forced turbulent wall jets. Thus, our previous work on wall jets in the proposed period consisted of three parts: the wall jet on a curved surface (including experiments on and theoretical models of the flow around a Coanda cylinder); the weak wall jet; and the coherent motion of the forced turbulent wall jet.

RESULTS AND DISCUSSION

1. The Turbulent Wall Jet Along a Convex Curved Surface

The experiments were carried out on the surface of a circular cylinder with a diameter of 203.2mm (Coanda cylinder). The slot width was varied from 2.3mm to 6mm. Both single and X hot-wire probes were used for velocity measurements. The hot-wire experiments were conducted at a Re_N number of 33,000 for comparison with existing results from the plane wall jet of Re 7000 (Zhou et al.1996). The jet separated beyond 230° as long as the Re number was high enough and the slot width to cylinder radius ratio was small enough. The main purpose of this investigation was to determine the effect of surface curvature on the development of a two-dimensional wall jet as compared to its plane counterpart.

Fig.3 shows the surface pressure distribution, where R the radius of the cylinder, b the slot width, p_o the plenum chamber pressure, p_s the static surface pressure and p_∞ the surrounding pressure. The surface pressure remains approximately constant up to 120° and a steep increase of surface pressure occurs thereafter.

Fig.4 is the streamline calculated from the measured velocity data. The flow grows gradually until a sudden growth occurs showing an approach to the separation, which matches very well to the pressure distribution. The corresponding streamwise development of the shape factor is also compared with the pressure distribution, which also shows the same phenomena related to separation. (Fig.5).

The mean velocity profiles for the upstream region $40^o < \theta < 120^o$ normalized with only one length scale and one velocity scale are compared with the plane wall jet in Fig.6a-c. The solid lines in the figures represent an averaged mean velocity profile for the plane wall jet. It is evident that even though the mean velocity profiles for the tangential component appear similar the normal component is not.

The development of y_2 and U_{max} are shown in figure 7 in a conventional way. All the data are well collapsed on a single line up to where separation occurs. In order to compare with the plane wall jet. They are shown again (Fig.8) in a scaling manner for plane wall jets which is governed by the jet momentum J and viscosity ν (Wygnanski et al 1992). The results from the plane wall jet are represented by straight dotted lines. The curved wall jet shows a larger spreading rate and a

faster velocity decay than its plane counterpart. It does not obey the scaling law for plane wall jets though their u-mean velocity profiles behave similar. It is believed that on the curved wall jet where centrifugal force and Coreolis force may play so important role that viscous force becomes no more dominant. Thus, only the data close to the nozzle, where viscosity is still dominant for the development of the jet, lie on the curve for the plane wall jet.

Figure 9 compare the streamwise and radial turbulence intensities for the plane and curved wall jet. The increasing of the radial turbulence intensities $\sqrt{v'2}$ for the curved wall jet can be regarded as a direct consequence of the increased turbulence production caused by the centrifugal forces. The increasing of tangential turbulence intensity should be due to increasing of production caused by the Coriolis force (Wilson & Goldstein 1976). The influence of the curvature on the Reynolds stress production and consequently the Reynolds stress distribution can also be seen in the measured data (figure 10). The effect of curvature on the mixing is significant since the value of the turbulent stress in the curved wall jet are one magnitude larger than the one in the plane wall jet.

Although important results have been obtained as mentioned above, the hot-wire techniques fail in certain regions where mean velocities are low and turbulence intensities are high, mainly in the outer layer with large inclination angles due to the strong entraining motion and in the separation region where reverse flow will be encountered. Thus, a Particle Image Velocimeter (PIV) was employed. The cross-correlation technique was applied for data processing procedure which is believed to be the better approach where there is reverse-flow.

Figure 11a shows a comparison of the hot wire and PIV measurements and Fig 11b is the color original of the PIV results. The hot wire data at an azimuthal angle of 200 degree from the nozzle pretends a fully attach flow while the averaged PIV data disclose already separation. Apparently, the PIV system will be a necessary tool to investigate the process of separation in the future.

Further more, the PIV technique was tried in a forced flow. Limited by the technique, the results to date were obtained from a lower velocity than the hot wire measurements, however, it showed its potential in discovering the instantaneous vortical structures. Fig.12 shows the vorticity contours in the forced flows. Three co-rotating strong vortical structures can easily be identified from the instantaneous vortisity contour (Fig.12a). The global effect of forcing can be seen from the time mean vorticity contour (Fig.12b). This part of work has just been started. Detailed structural observation is expected to be one of the major works in our future study.

2. The theoretical model of the mean wall-jet flow around Coanda cylinder

The effect of curvature on the flow stability is an important subject for the active separation control. As the first step, the mean flow similarity of the flow around the curved surface was investigated theoretically. The conventional boundary-layer assumption was applied to the momentum equations. This implies that the wall jet thickness at any location is small in comparison with the streamwise distance or with the characteristic radius of curvature. One can

chose the ratio of the wall jet thickness to the radius of the cylinder $\varepsilon = Y_{m/2}/R$ as a small parameter in the order-of-magnitude analysis. When ε tends to zero the jet flow is the plane wall jet for which similarity was obtained by Wygnanski et al. (1992). In contrary to the plane wall jet, the wall jet flowing along the curved surface has an external length scale, the radius of the cylinder R which has to be taken into account due to the 'geometrical effect'. We assume that the bulk of the flow under investigation is self-similar and described analytically by the following power laws:

$$\left[U_m \Big/ \left(\frac{J}{R}\right)^{1/2}\right] = A_u\left[(\theta - \theta_0)\right]^n, \quad \left[Y_{m/2}/R\right] = A_r\left[(\theta - \theta_0)\right]^m. \tag{1}$$

where U_m, $Y_{m/2}$ are the local maximum velocity and the distance measured from the wall to the location at which the mean velocity decreases to 1/2 of its local maximum value in the outer part of the flow respectively; R and θ are the radius and the angular distance around the cylinder, respectively; $J = bU_j^2$ is the momentum flux of the jet in the slot; θ_0 is the angle measured from the jet exit to apparent origin.

Making use of (1), the non-dimensional variables can be introduced as

$$\xi = (\theta - \theta_0), \quad r/Y_{m/2} = \frac{1}{\varepsilon} + \eta \tag{2}$$

where $\eta = (r - R)/Y_{m/2}$ is the dimensionless distance from the surface and $\varepsilon = Y_{m/2}/R$ is the small parameter discussed above. To solve the problem we will try to close the equations of motion with the help of an eddy viscosity model. The eddy viscosity is introduced by the relation

$$\nu_t = \varepsilon\left(U_m Y_{m/2}\right)\xi^{-1}(1+\varepsilon\eta)^{-1}\sum_{k=1}\left[\kappa_k(\xi)\eta^k f^{(k)}\right] \tag{3}$$

where the stream function is used $\Psi = Y_{m/2}U_m\, f(\eta)$ since the flow of interest is two dimensional and $f^{(k)} = \partial^k f/\partial\eta^k$. Substituting (3) into the equations of motion and keeping the terms of leading order ε, the set of ordinary differential equations is obtained as:

$$P_1' = \frac{\left(f'^2 + \varphi_0\right)}{(1+\varepsilon\eta)} + \left(\mathrm{Re}_l\,\xi\right)^{-1}\left[(m-n)f'' + m\eta f'''\right],$$

$$\left\{\left[A(\xi)(1+\varepsilon\eta) + \sum_{k=1}\kappa_k\eta^k\, f^{(k)}\right]f''\right\}' + (n+m)ff'' - nf'^2 - \Phi_0(\eta,\xi) = 0 \tag{4}$$

where

$$A = \xi^{(1-2m-n)} \Big/ \left(\sqrt{2} A_u A_r^2 \,\mathrm{Re}\right)$$
$$\Phi_0 = \xi \frac{\partial \varphi_0}{\partial \xi} + 2n\varphi_0 - m\eta\varphi_0 \,' \,. \tag{5}$$

and $P = P_\infty + \varepsilon U_m^2 \, P_1(\eta)$, $\overline{u_\theta}'^2 = U_m^2 \, \varphi_0(\eta, \xi)$ are pressure and normal component of the shear stress and Re is the Reynolds number introduced by Newman (1961):

$$\mathrm{Re} = \left\{(\mathrm{P}_0 - \mathrm{P}_\infty)\mathrm{bR}/\rho\nu^2\right\}^{1/2}. \tag{6}$$

Making use of n, m, A_u, A_r from the experiment, one can solve the problem (4) with the shooting procedure to meet the fitting conditions $f'(\eta_m) = 1$ and $f'(1) = 0.5$. The comparison between the theoretical profile and the measured one at $\mathrm{Re} = 3.3 \cdot 10^4$ for slot width $b = 2.34\ mm$. is shown in Fig. 13.

The dashed line represents the theoretical velocity profile obtained with the semi-empirical model without taking into account the term $\Phi_0(\eta, \xi)$ in (4) while the soled line with the normal stress. The latter is in good agreement with the measured velocity profile.

3. Weak wall-jet.

The experiments were carried out in a close-loop wind tunnel. The wall jet facility can be seen in Zhou & Wygnanski 1993. Single-wire probes were used for velocity measurements. In all, nine sets of weak wall jets were measured, including various Jet Reynolds number, various velocity ratio between jet velocity and external velocity, various jet exit thickness and various momentum thickness of the upstream boundary layers.

A weak wall jet is one in which the tangential momentum added to the flow is small compared to the momentum deficit in the boundary layer. Fig.14 shows four sets of mean velocity profiles with order of increasing the ratio between the momentum deficit in the boundary layer and the momentum added by the jet Uj^2b. When the ratio is less than 0.035 (Fig.14a) a typical strong wall jet profile is shown where there is no velocity minimum. Fig.14 b-d show three sets of weak wall jets where the momentum ratio is equal or greater than 0.035. A general feature of the weak wall jets can be seen in the figure, i.e. they usually contain a mean velocity minimum to start with. However, two different classes of weak wall jets can be identified: one tends to a strong wall jet type flow in the downstream location after the velocity minimum disappears (Fig.14b) and the other, the velocity deficit (a wake) remains until it tends to a skewed boundary layer flow (c and d). For the first category, in the region after the velocity minimum disappeared the mean velocity profiles are composed of two shear layer regions and can be collapsed when two velocity scales and two length scales are used for normalization, which is similar to the strong wall jet (Fig.15). However, for the second category, in the region where the velocity minimum plays important part, the mean velocity profiles are composed of three shear layer regions (Fig.14). In these

regions, three length scales and three velocity scales have to be adopted to obtain a successful normalization (Fig.16).

The above normalization procedures predicts an important new phenomena in the weak wall jet. While there are only two instability modes in the first category, there should be three instability modes in the second type, including one viscous mode related to the boundary layer type of instability and two invicid modes related to the two inflection points in the middle and outer region of the flow. Their relevant vortical structures will coexist and couple to each other. A search of the possible existence of the three instability modes for the second type weak wall jet was made by turbulence intensity, spectra and the phase-locked measurements.

Fig.17 shows the normal distribution of turbulence intensity. The mean velocity profiles are also plotted in these figures for comparison. It is apparent that there are three peak intensity in the three shear layer regions. The deviation of the intensity peak from the maximum shear is believed to be due to advection and diffusion effects.

A set of spectra are shown in Fig.18. No obvious peak frequency could be found in the unforced case. Thus, forcing with various frequency was applied to search for the different instability mode. The forcing amplitude was kept low (0.75%) so that no apparent skewing of the mean velocity profiles would occur. The amplitude and phase distribution of the disturbances under forcing were obtained by the phase-locked ensemble averaging procedure. As indicated in Fig.19, forcing at 104Hz caused a major peak of amplitude at the wall region, which corresponds to a viscous dominant mode or the boundary layer mode. The phase information was also recorded as reference (Fig.20). Forcing at 75Hz, however, the peak at the inflection point in the middle region became outstanding (Fig.21) though there are still peaks close to the wall, which indicates the existence of one of the invicid mode or the middle mixing layer mode. The influence of forcing on the peaks expected to occur at the outer inflection point or the outer mixing layer mode is not so apparent. From the later discussion in section 4, it will be clear that it is because of the strong phase jitter in the outer layer which smeared out the phase locked coherent intensity.

A related investigation on the global effect of forcing on the flow was made by skin friction and wall jet thickness measurements. Skin friction reduction means a reduction of drag and skin friction increase could imply a potential to prevent separation or increasing of the heat transfer on the wall. Further more, a thickening of total layer could imply an enhance of mixing or potential increasing of heat transfer across the flow. These results are shown in the following figures. Fig.22 shows the skin friction reduction along the streamwise direction, where the forcing frequency corresponding to the viscous mode was introduced. The maximum reduction was about 30% in this case. Fig.23 shows the thickening of the wall jet under forcing while the mean velocity profiles remain almost unskewed.

4. Coherent motion in forced turbulent wall jets.

Our recent publication (Zhou et al 1996) represents in part experimental results gathered during the past two years. Entirely novel, however, is the section dealing with the identification of

coherent structures in the forced turbulent wall jet and the energy budget which is based on triple decomposition of the motion into steady, coherent and random components.

Coherent structure, as a concept, has been accepted for decades by most of the scientists involved in turbulence research. However, the double decomposition procedure suggested by Reynolds, in which all quantities in the equations of motion are decomposed into mean and fluctuating components, cannot reveal anything about the nature of coherent structures. The decomposition of each instantaneous variable into a steady component, a fluctuating coherent component, and a random one was analyzed by Hussain (1983). It is the formalism which enabled the author to derive the equations of continuity, momentum, vorticity and kinetic energy for all three constituents of the motion. These equations appeared to be well suited for gaining insight into the evolution of coherent structures and the energy exchanges which take place among all the components comprising the motion. However, the definition of the coherent constituents is ambiguous even in the presence of periodic excitation which provides a phase reference for the reduction of the data. A large body of experimental evidence suggests that a simple, phase-locking and ensemble-averaging procedure does not represent the coherent structures correctly because it encompasses but a small fraction of the energy contained in the coherent eddies. Furthermore external excitation not only provides a reference phase but it also modulates the flow and interacts with it. To some extent it reorganizes the coherent motion existing naturally in the flow and enhances it as well as producing abundant frequency components including the frequencies lower than the forcing frequency. Thus coherent motion should not be synonymous with phase-locked motion.

The various techniques used to identify the coherent constituents of the turbulent motion can be divided into two categories. In one category the phase relationship (e.g. the phase-locked ensemble-averaging procedure) is regarded as the dominant feature; in the other, the spatial scales (or frequencies) dominate. The dynamical system approach indicates that the attractor-dimension required to represent a complex dynamical system which captures all of the relevant spatial scales is enormous. To solve such a problem is both numerically delicate and computationally expensive. Advances in such areas will most probably necessitate a dramatic reduction in complexity, which may inadvertently remove some essential degrees of freedom. A rational reduction of the degrees of freedom can be facilitated by the experimental discovery and unambiguous definition of coherent structures. Thus, the low-dimensional computational techniques for flow simulation based on an understanding of the coherent structures are an important field to explore.

It has been found in the forced turbulent wall jet that the major portion of the instantaneous time signals can be reproduced by a few of (order of 5) Fourier components (Fig.24). It was also shown that, in the case of the wall jet, by recovering the recorded phase jitter, this limited number of components can re-establish the major feature of the broad band spectra obtained from the total velocity fluctuations (Fig.25), thus supports the reasonable physics. So, the key point of our method is to apply the pattern recognition technique in the time domain for all the individual Fourier components of interest, i.e. applying the Fourier transformation to the individual realizations of the corresponding patterns instead of the entire duration of the signal.

For this purpose, the time series are subdivided into segments containing the minimum number of waves sufficient for the pattern of interest to be conserved, for example, one wave in each segment representing the fundamental (forcing) frequency and its higher harmonics, two waves in each segment for the subharmonic frequency, four waves for the second subharmonic frequency, etc. Only then is the ensemble averaging procedure used. This "chopping" of signals is necessary since any longer segmentation will smear out a portion of the "coherent" pattern because of jitter.

The remaining problem in this procedure is the remaining jitter in the mean velocity since the mean value will vary from segment to segment. Actually, it stems from the residue of the data processing procedure and it accumulates the effect of all the components having frequencies lower than the truncation frequency. Physically, this part can be further divided into coherent and random portions. However, in practice we can regard the magnitude of the jitter as another part of the random motion, as long as we are confident of the fact that the number of Fourier components chosen to represent the coherent motion is sufficient. One should therefore start from the lowest frequency of interest, and chop the signal to account for the corresponding largest structure, subtract it from the total signal, then re-chop the segment and proceed to the second lowest frequency, etc. Fig.26 shows some results obtained by the new procedure (a,c,d) and the apparent improvement on educing the coherent motion compared to the conventional phase-locked ensemble averaging procedure (Fig.26b).

The disregard for jitter in the conventional definition of the average intensity of the phase-locked signal smears out a significant portion of the coherent intensity. It is the main reason why an energy balance related to the coherent motion can not be constructed based on this technique. In stead, the new technique enabled us to construct a reasonable energy budget for the wall jet in which the coherent part plays a dominant role. This procedure was used to a strong wall jet and was for the first time able to obtain a successful energy balance by the triple decomposition (Fig.27).

Based on the above success, this procedure was tested also to the forced weak wall jet to explore the other invicid instability mode. Fig.28 shows that there really is another peak at the outer inflection point which is at least of the same importance as the peak at the middle inflection point under forcing frequency of 75 Hz. Thus, the other invicid mode was revealed by the new procedure. Combining with Fig.20b where shows a phase jump of 180^{o} at the velocity minimum, it can be seen that the two invicid modes are strongly coupled. They oscillates in a way that the disturbances at the different sides around the velocity minimum are of opposite sign and with approximately the same amplitude, i.e. these two modes are almost combined to be one anti-symmetrical mode relative to the velocity minimum in this case.

Further development of this decomposition procedure is still under way.

CONCLUSION

1. Hot wire data and PIV observations have been obtained on the Coanda cylinder which show the strong influence of curvature and of the pressure gradient on the wall jet. New structures were

also observed in the forced case which is expected to have important influence on the separation control.

2. A theoretical model was established for the mean flow around the Coanda cylinder, which will be an important tool in the further stability studies. The calculated the mean velocity profiles were shown in good agreement with the measured data.

3. Two types of weak wall jets have been observed. Different number of length scales and velocity scales were found for the two categories. Normalization of the mean velocity profiles were found successful. The related stability modes indicate important physical background for the future stability studies and for separation control.

4. A novel technique for identification of coherent motions was developed which can eliminate the influence of phase jitter and discover much more coherent energy than the conventional phase locked ensemble averaging technique. Based on the new technique, a coherent energy budget was for the first time established reasonably. This technique will be applied to explore the function of coherent motion in the separation control.

REFERENCES

Hussain, A.K.M.F.: Coherent structures --- reality and myth. Phys. Fluids, Vol.26, pp.2845, 1983.

Newman, B.G.: The deflexion of plane jets by adjacent boundaries --- Coanda effect. in "Boundary Layer and Flow Control", Ed. Lachmann,G.V. Pergamon Press, pp.232, 1961.

Seifert, A; Bachar,D; Koss,D.; Shepshelovich,M; Wygnanski,I.: Oscillatory Blowing: A tool to delay boundary-layer separation. AIAA Journal Vol 31, No.11 Nov. 1993, pp.2052-2060.

Wilson, D.J. and Goldstein,R.J.: Turbulent wall jets with cylindrical streamwise surface curvature. J.Fluid Eng. Vol.98, pp.550-557, 1976.

Wygnanski, I.; Katz,Y. and Horev,E.: On the applicability of various scaling laws to the turbulent wall jet. J.Fluid Mech. Vol. 234, pp. 669-690, 1992.

Zhou, M.D. and Wygnanski,I.: Parameters governing the turbulent wall jet in an external stream. AIAA J. Vol.31, pp.848-853, 1993.

Zhou, M.D.; Heine,C.; and Wygnanski,I.; The effects of excitation on the coherent and random motion in a plane wall jet. J.Fluid Mech. Vol.310, pp.1-37

LIST OF PUBLICATION

1. Neundorf, R.; Zhou, M.D. & Wygnanski, I.: Flow of a wall-jet around a circular cylinder --- the Coanda effect revisited. The American Physical Society meeting in Atlanta, Nov. 1994.

2. Zhou, M.D. & Wygnanski, I.: A quantitative determination of the large coherent structures in the wall jet. The American Physical Society meeting in Atlanta, Nov. 1994.

3. Zhou,M.D.; Weidemann,M.; Wygnanski, I.: Experimental studies on the 2D turbulent weak wall jet. The American Physical Society meeting , Irvine, CA, Nov. 1995.

4. Zhou, M.D.; Heine,C.; and Wygnanski,I.; The effects of excitation on the coherent and random motion in a plane wall jet. J.Fluid Mech. Vol.310, pp.1-37, 1996.

5. Neundorf, R.: Turbulent wall jet along a convex curved wall, Master Thesis for University of Arizona and Technical University Berlin. 1995.

6. Weidemann,M: The weak wall jet, Master Thesis for University of Arizona and Technical University Berlin. 1996.

ATTACHED PAPER:

Zhou, M.D.; Heine,C.; and Wygnanski,I.; The effects of excitation on the coherent and random motion in a plane wall jet. J.Fluid Mech. Vol.310, pp.1-37.

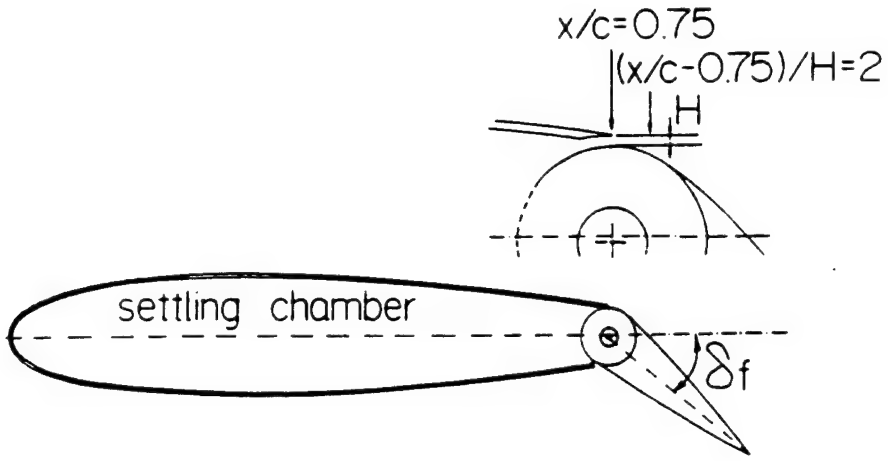

Fig.1 A sketch of the flapped NACA 0015 airfoil.

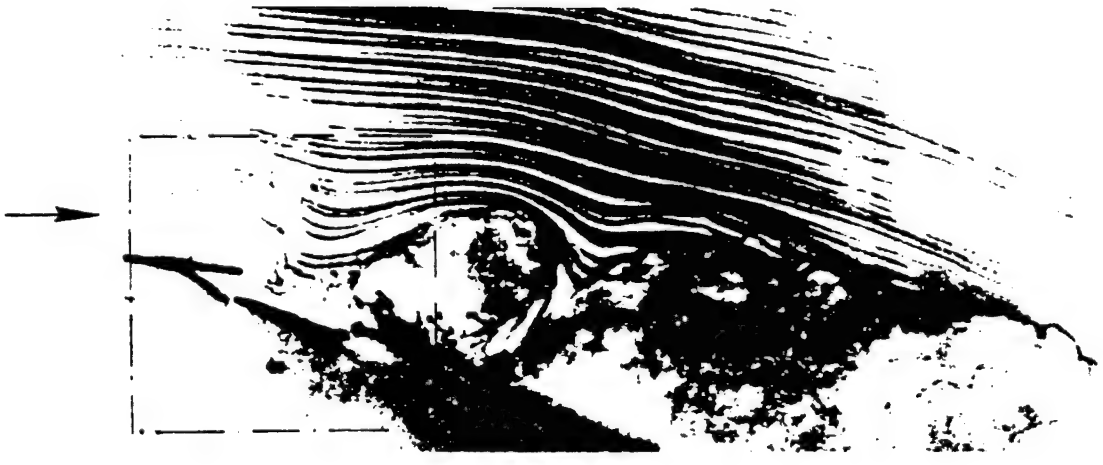

Fig.2 The flow visualization of the flow on the top surface with forcing.

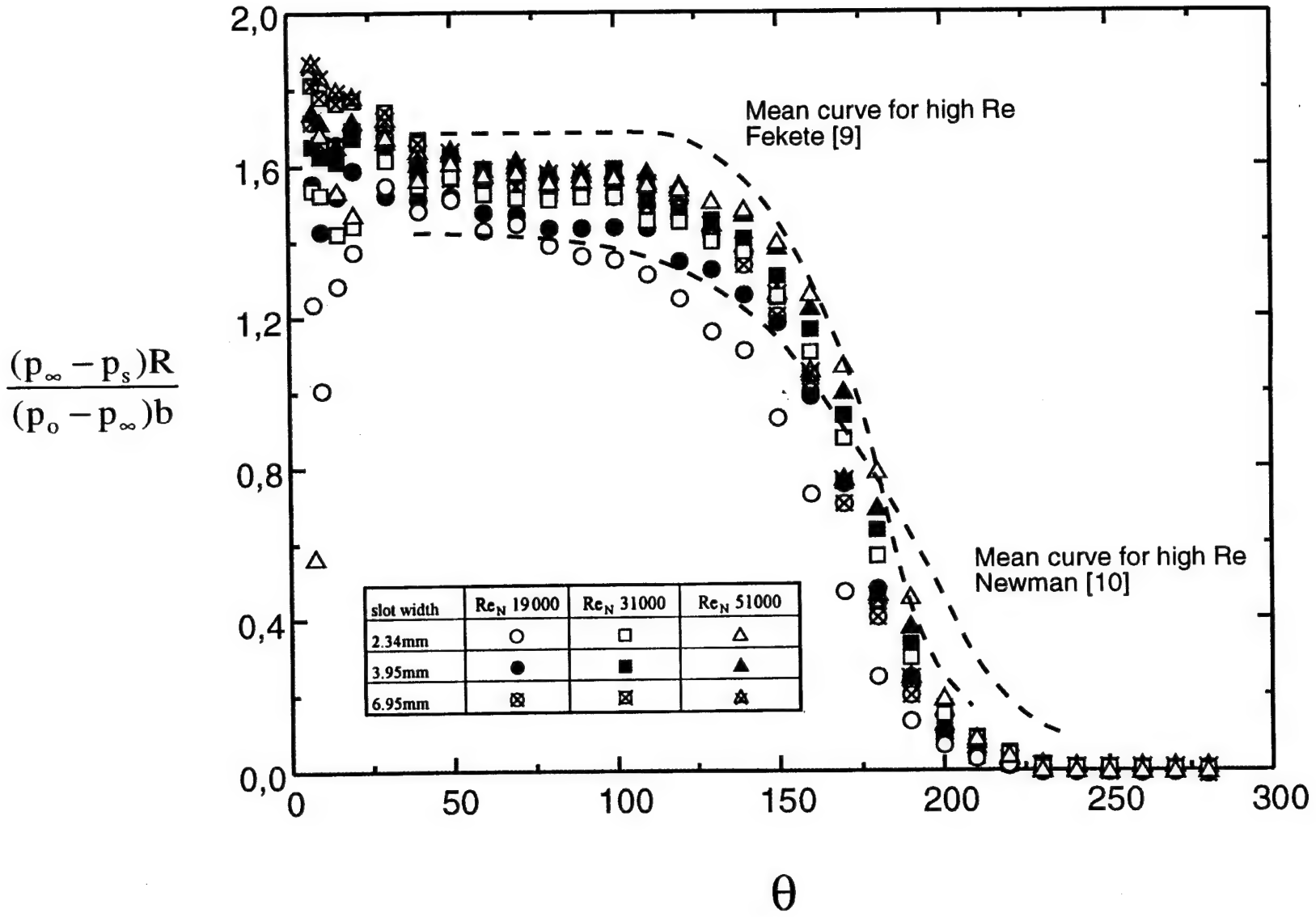

Fig.3 The surface pressure distribution on the Coanda cylinder.

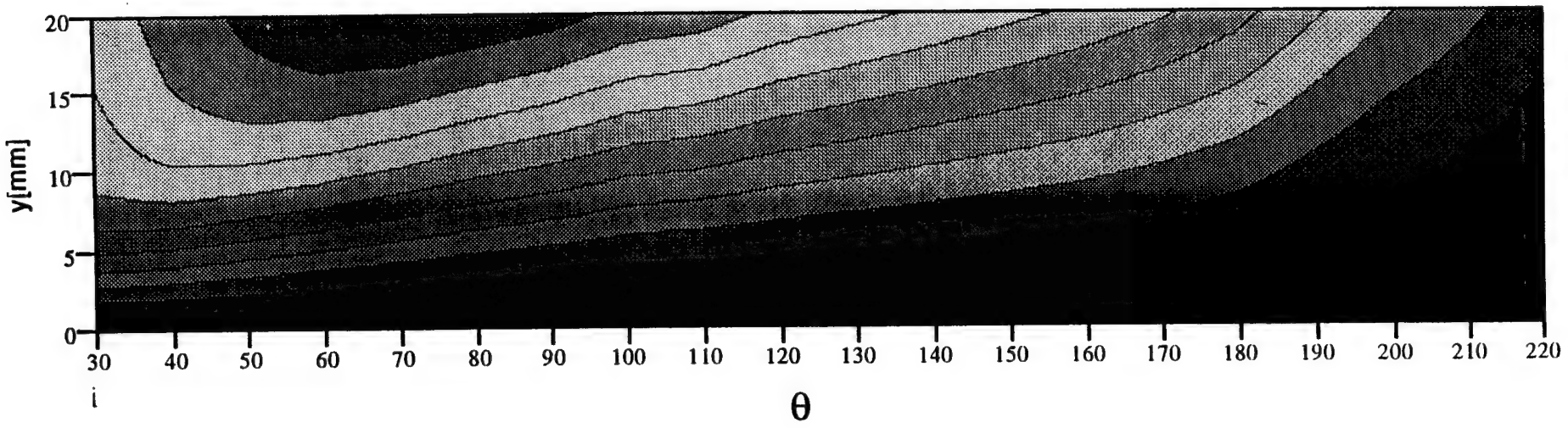

Fig.4 The mean streamlines around the Coanda cylinder calculated from the measured velocity field.

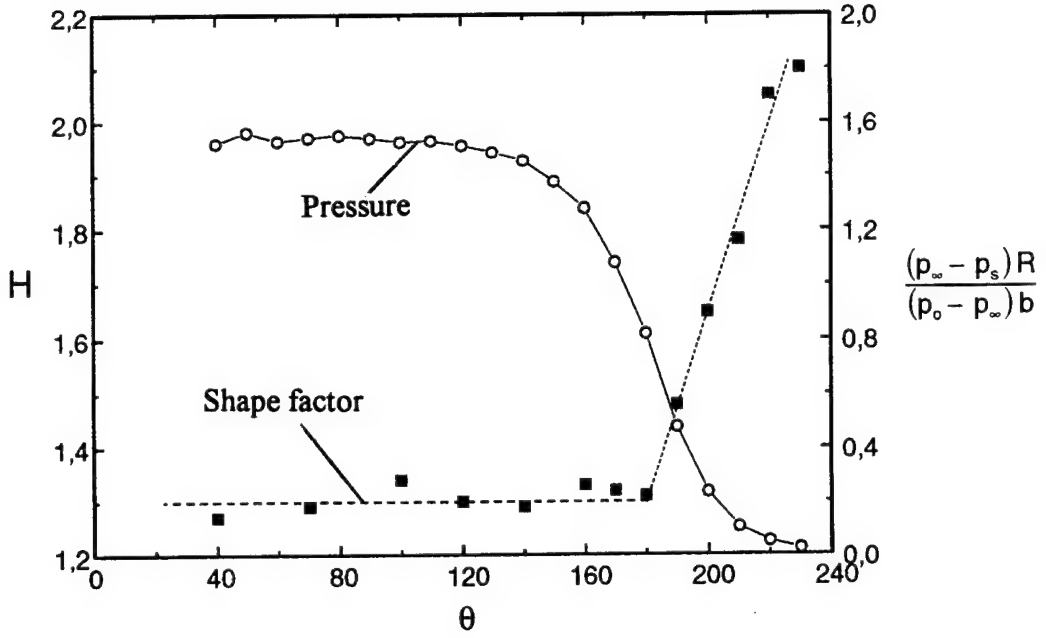

Fig.5 The streamwise distribution of the shape factor compared with the pressure distribution.

Fig.6 The mean velocity profiles on the Coanda cylinder.
a. streamwise velocity component, total layer.

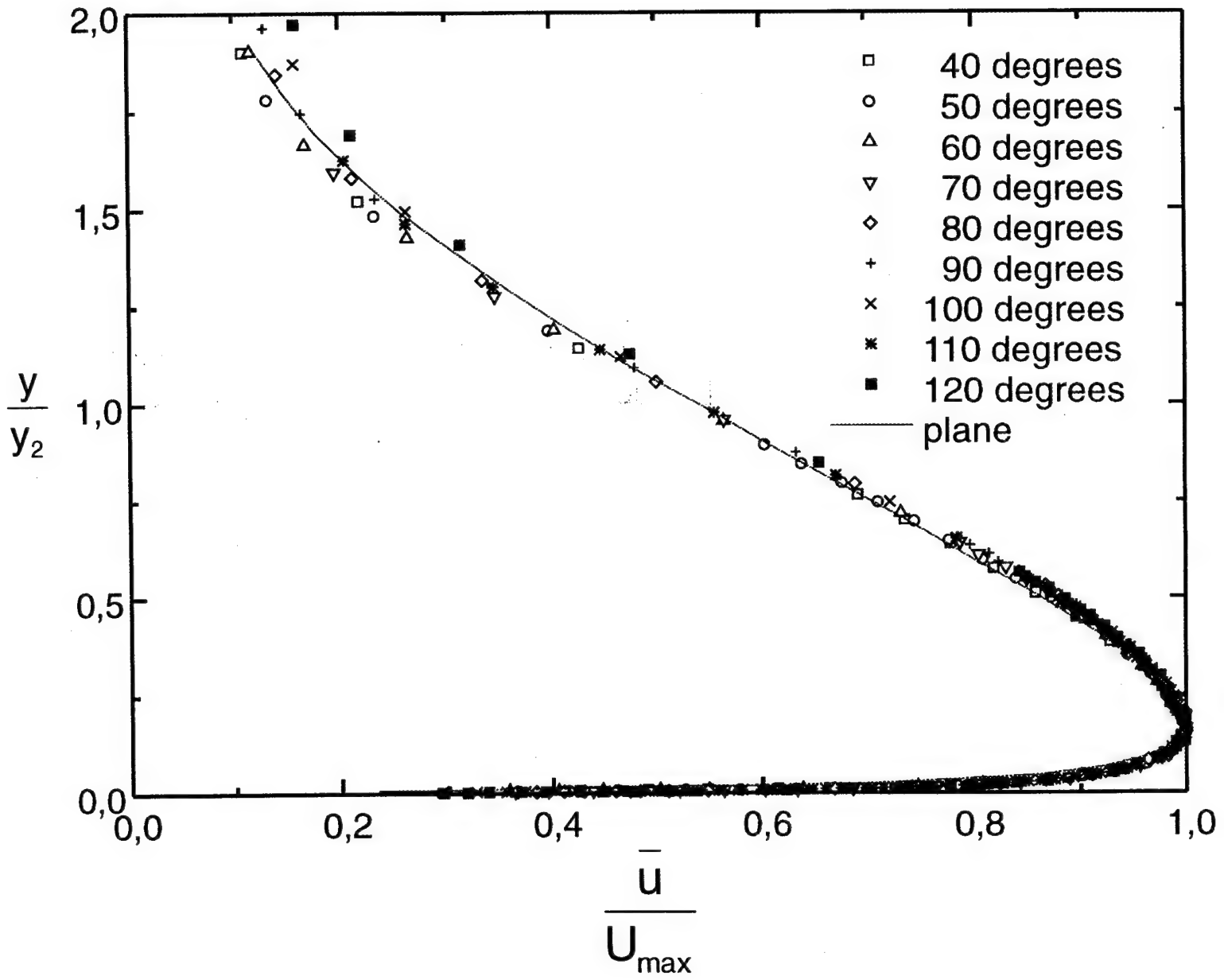

Fig.6 The mean velocity profiles on the Coanda cylinder.
b. streamwise velocity component, inner layer.

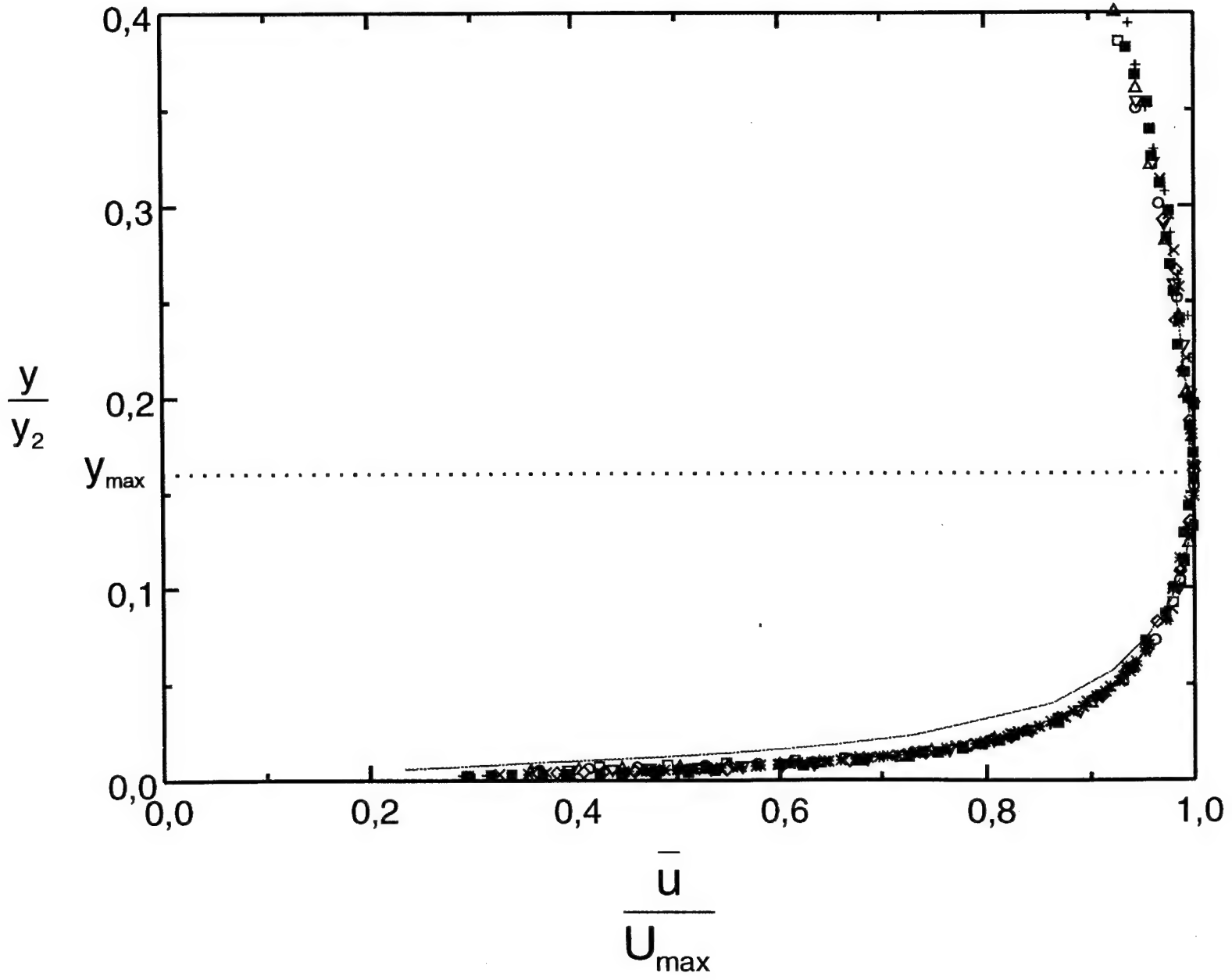

Fig.6 The mean velocity profiles on the Coanda cylinder.
c. radial velocity component.

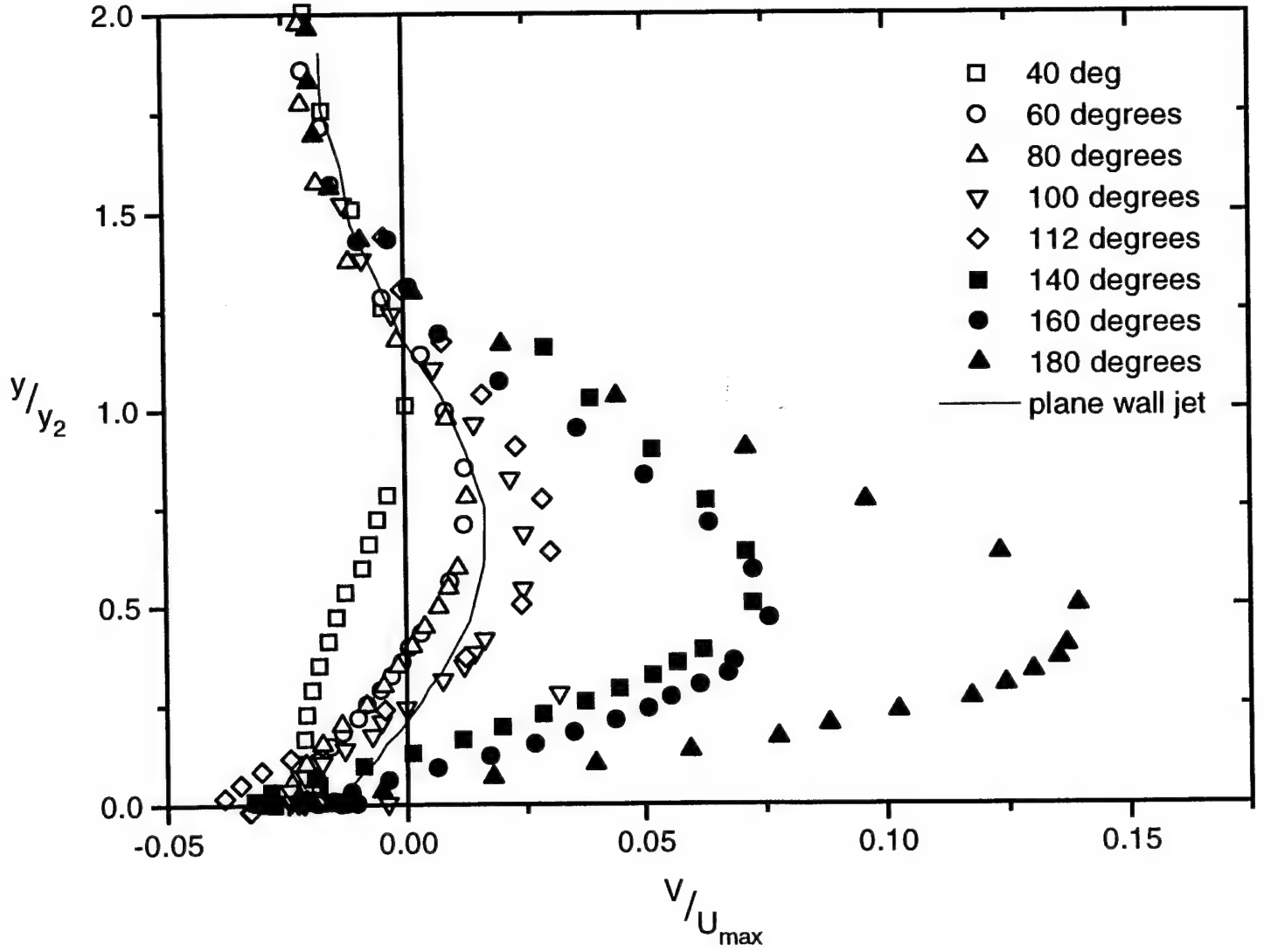

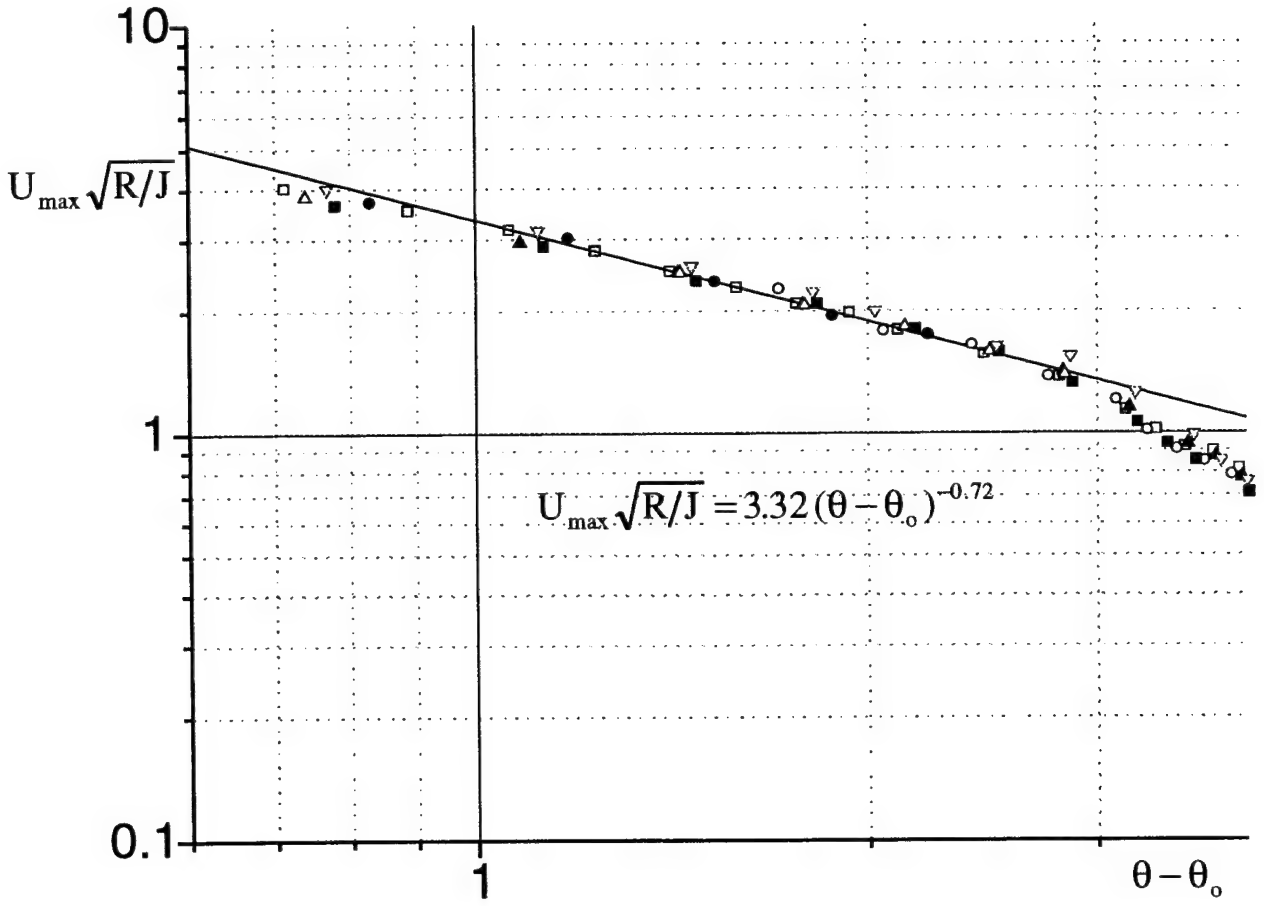

Fig.7 Scaling of the velocity scale and length scale in the ordinary manner.
a. velocity scale.

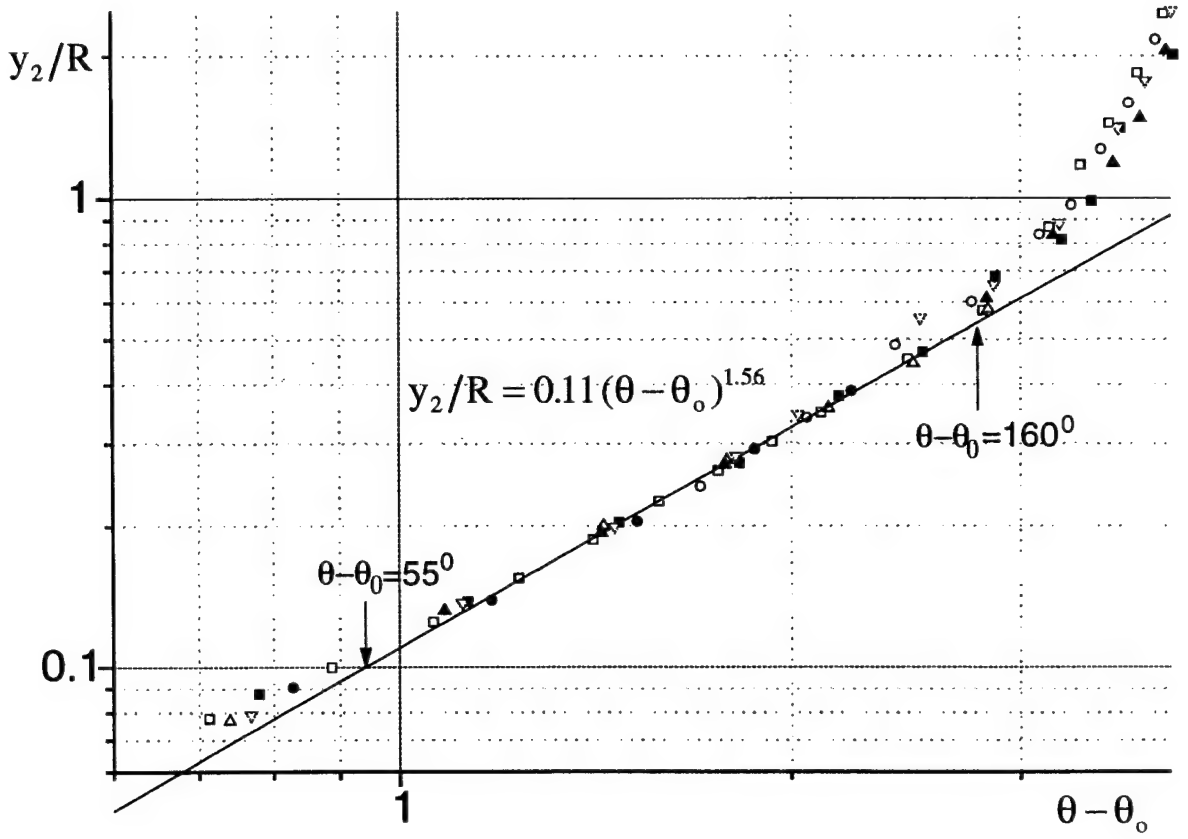

Fig.7 Scaling of the velocity scale and length scale in the ordinary manner.
b. length scale.

Fig.8 Scaling based on the jet momentum and viscosity.
a. velocity scale.

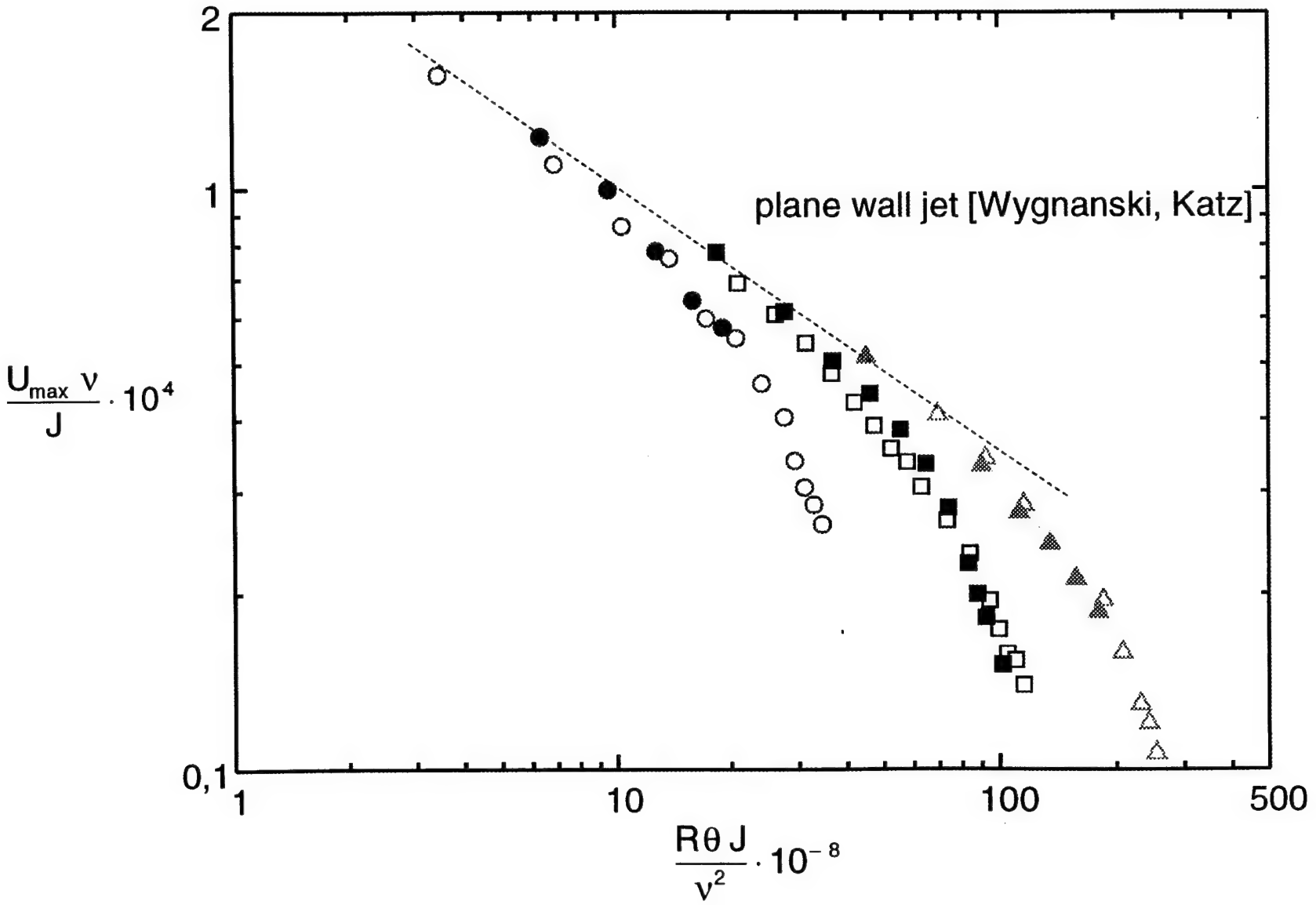

Fig.8 Scaling based on the jet momentum and viscosity.
b. length scale.

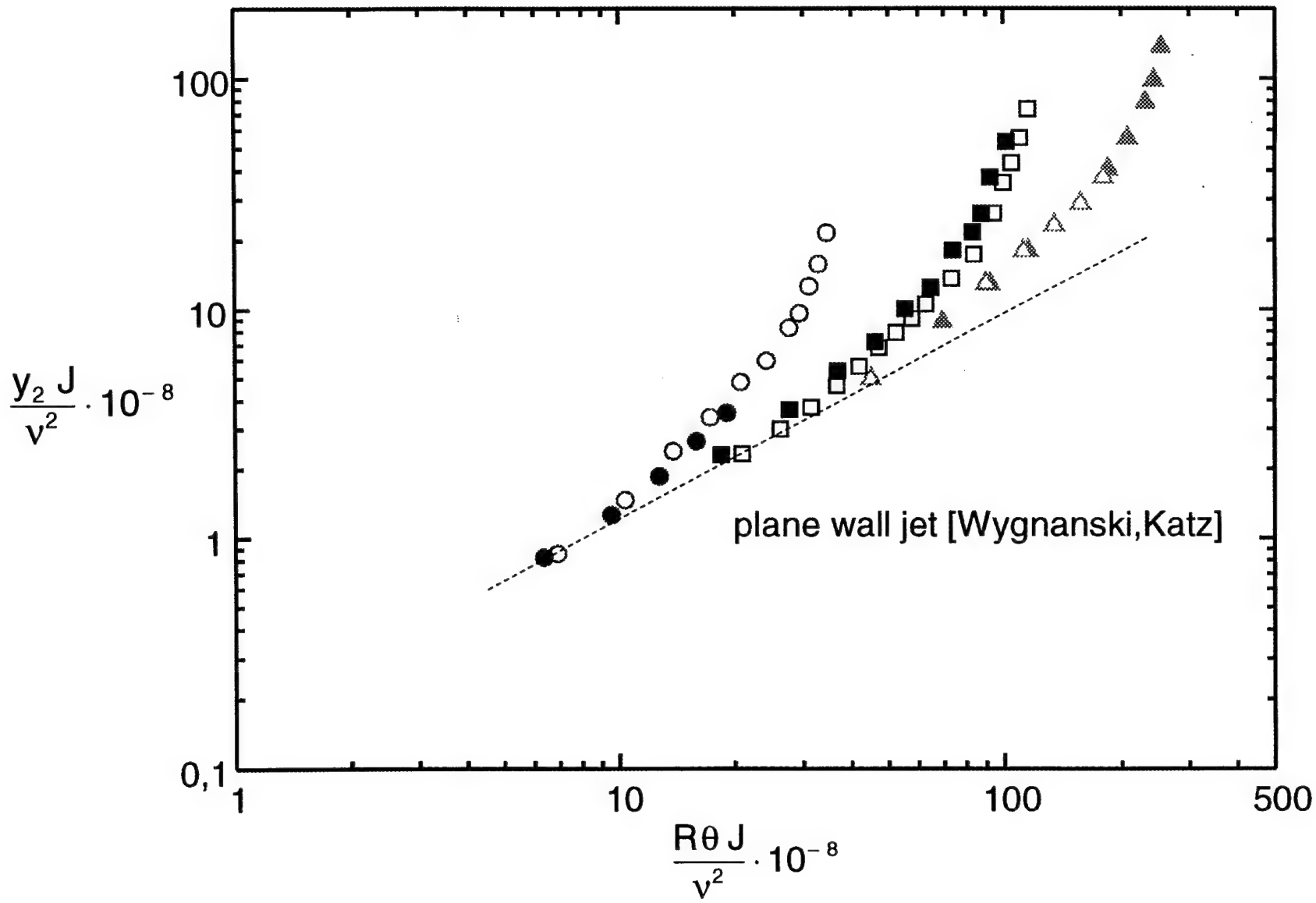

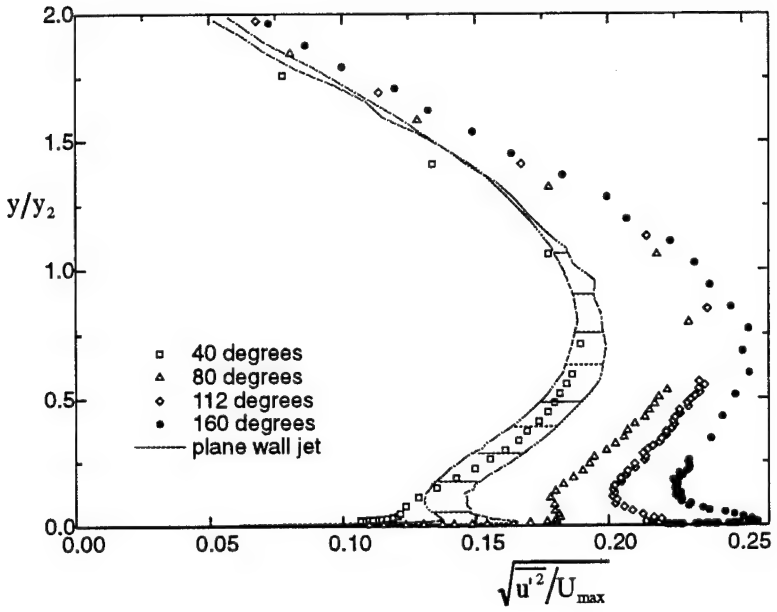

Fig.9 Distribution of the turbulence intensity.
a. streamwise component.

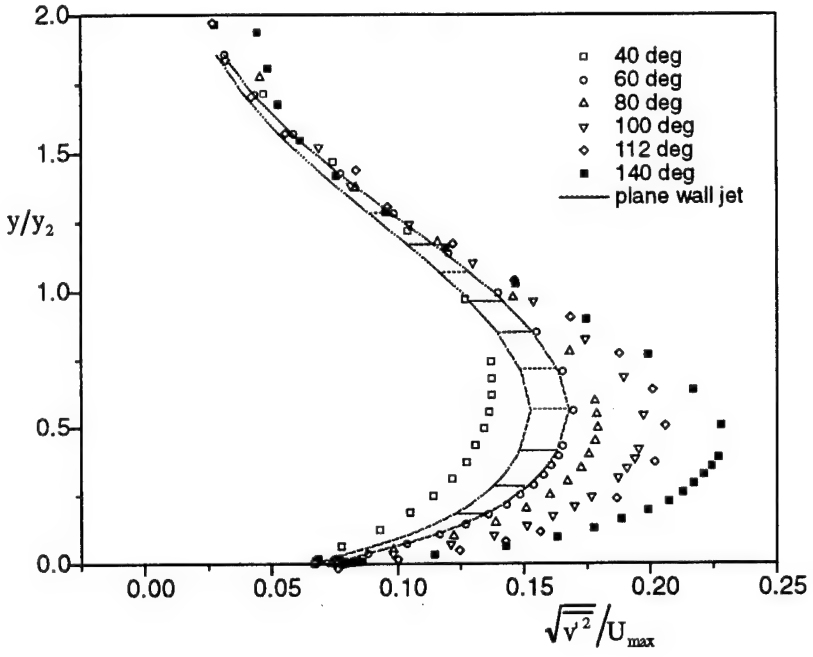

Fig.9 Distribution of the turbulence intensity.
b. radial component.

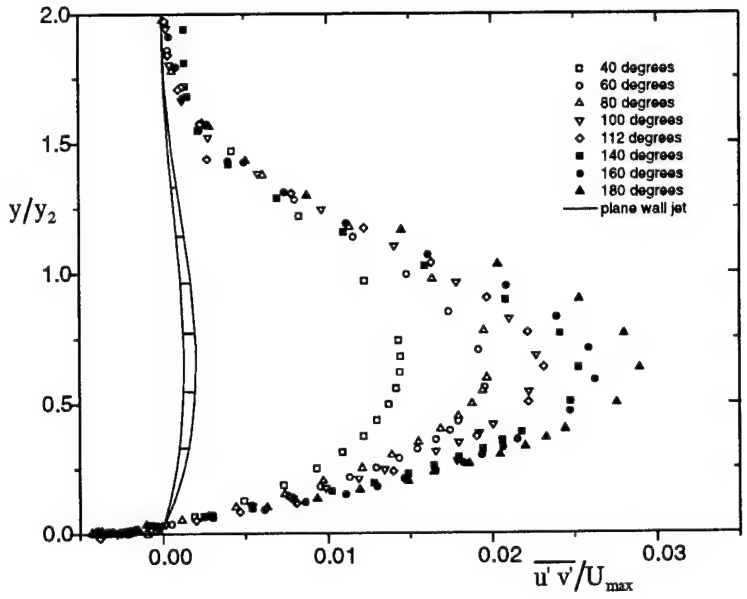

Fig.10 Distribution of the Reynolds stress.

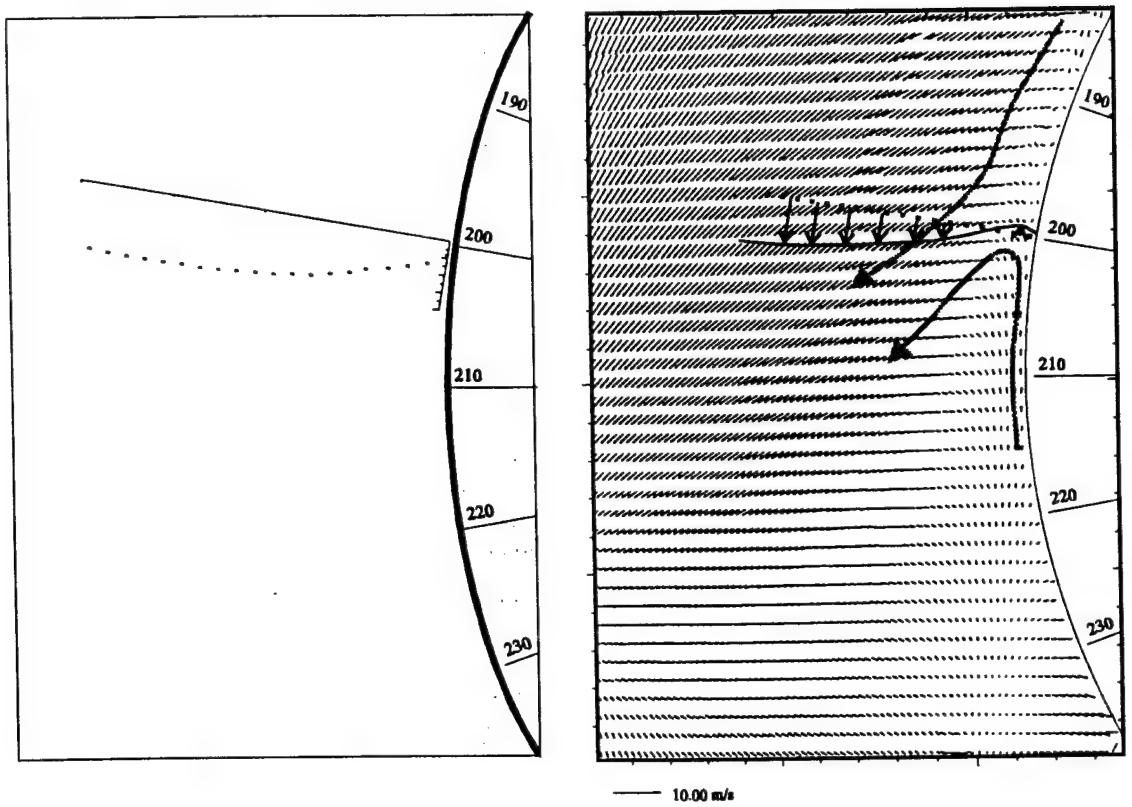

Fig.11 The mean velocity field obtained by the PIV with no forcing.
a. compared to the mean velocity profile measured by the hot wire.

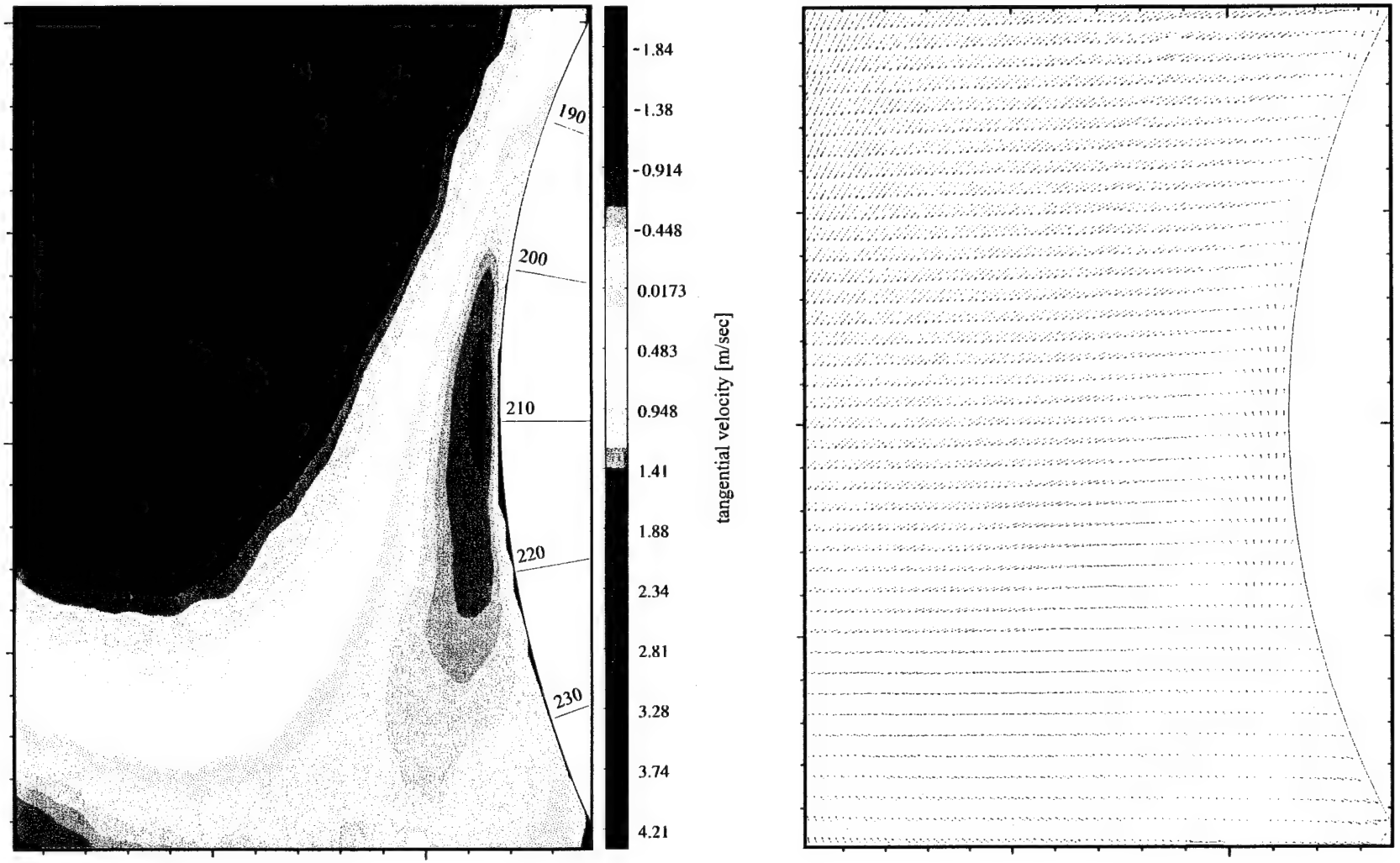

Fig.11 The mean velocity field obtained by the PIV with no forcing.
b. the mean velocity field in vector form and in map form.

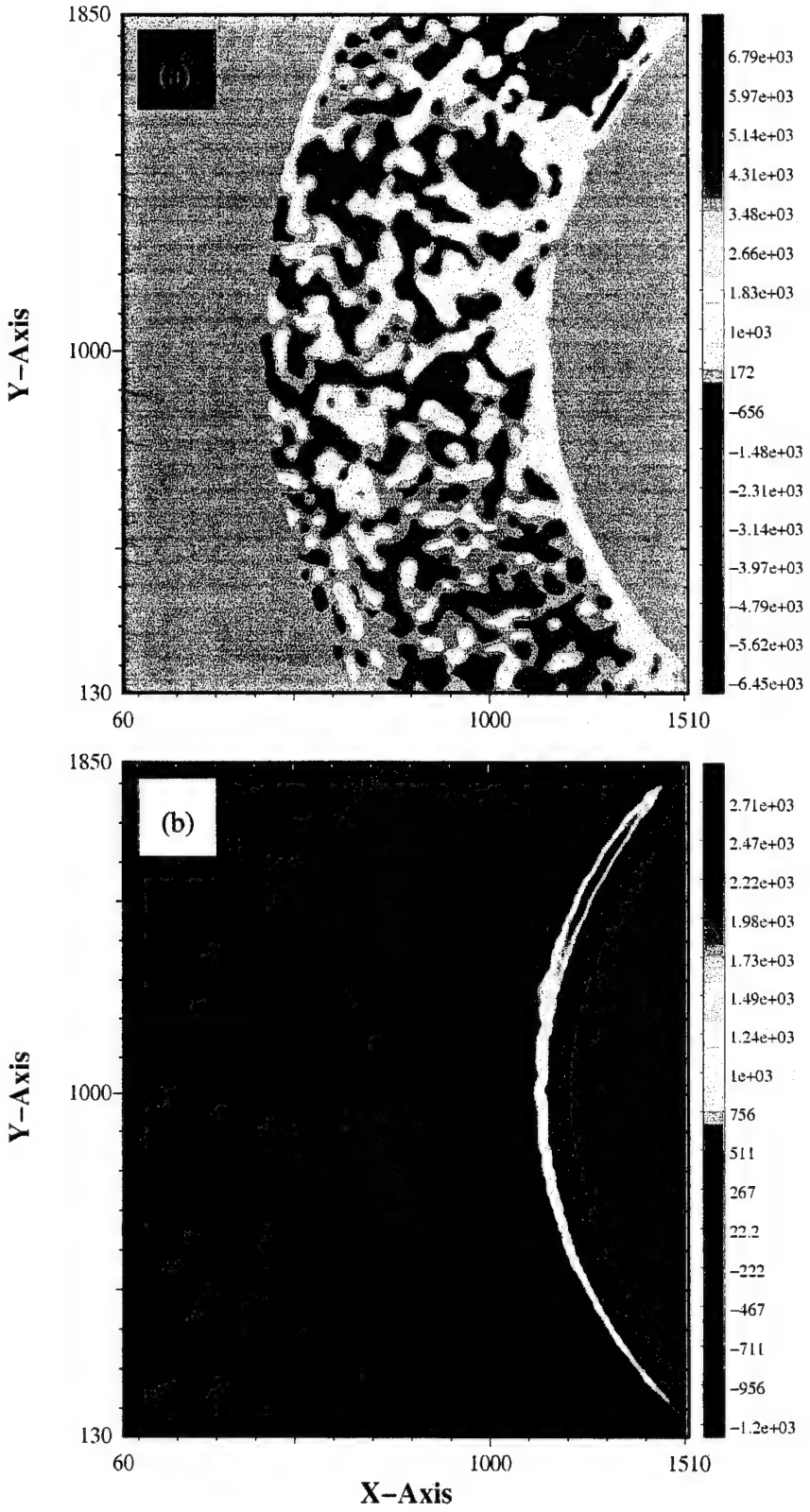

Fig. 12 The vorticity contours of a forced flow around the Coanda cylinder.
a. an instantaneous realization.
b. the time mean result.

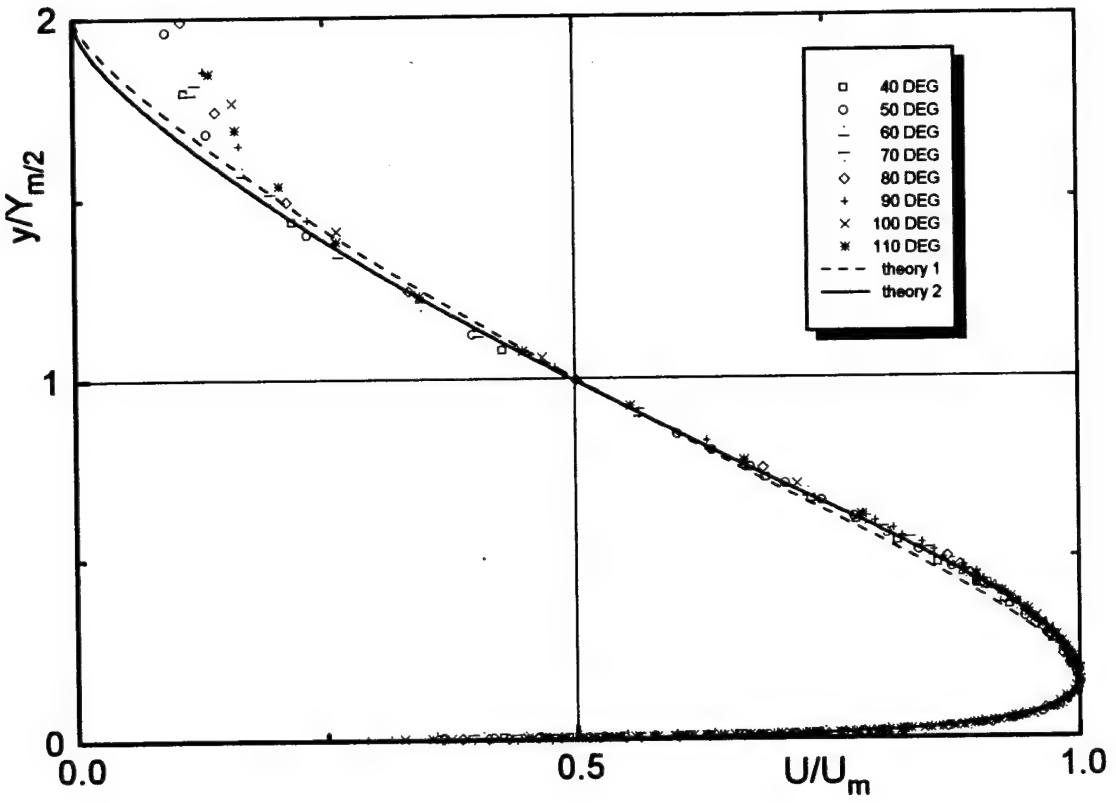

Fig.13 Comparison of the mean velocity profiles between measured data and the theoretical calculation.

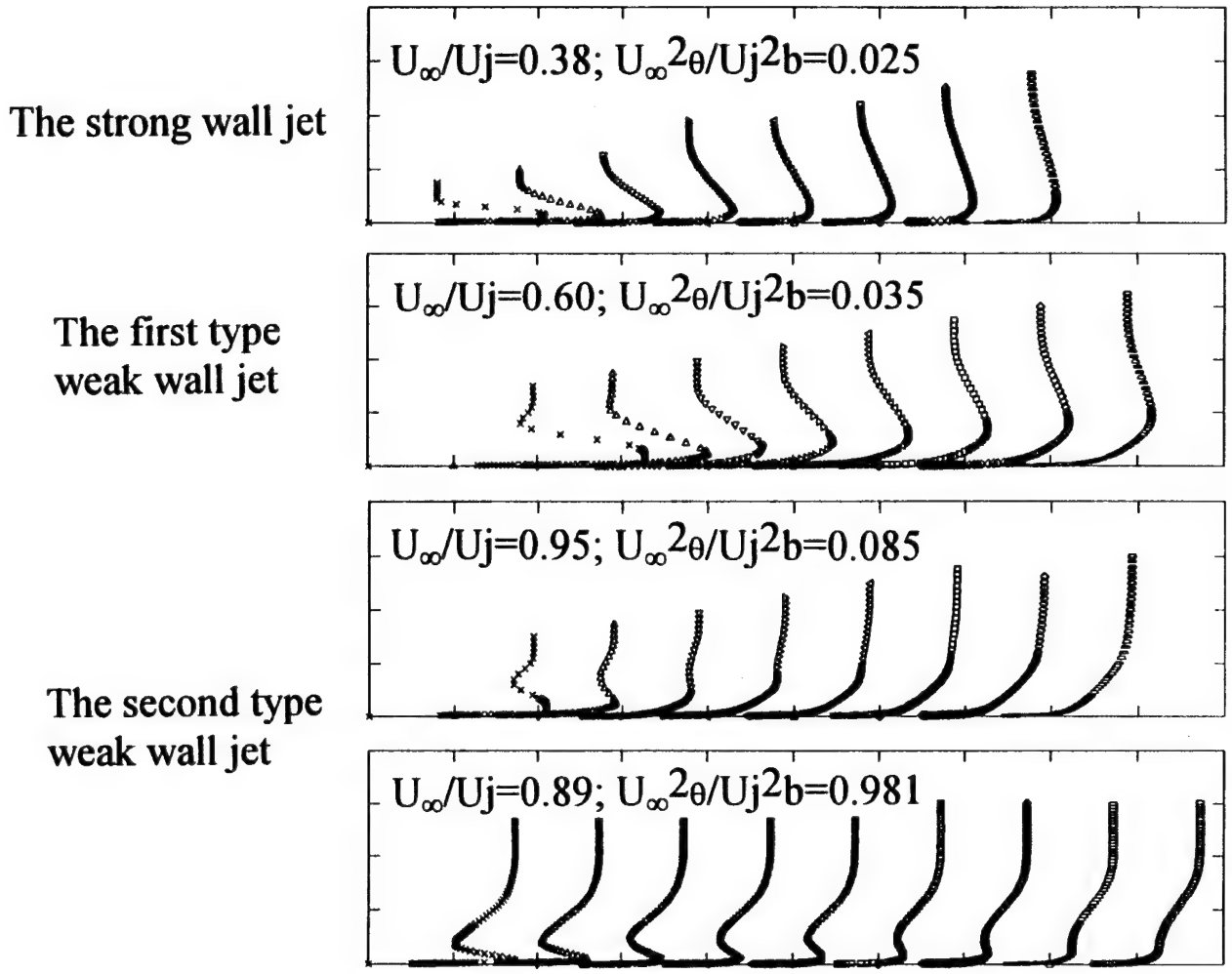

Fig.14 Mean velocity profiles of the typical wall jets.

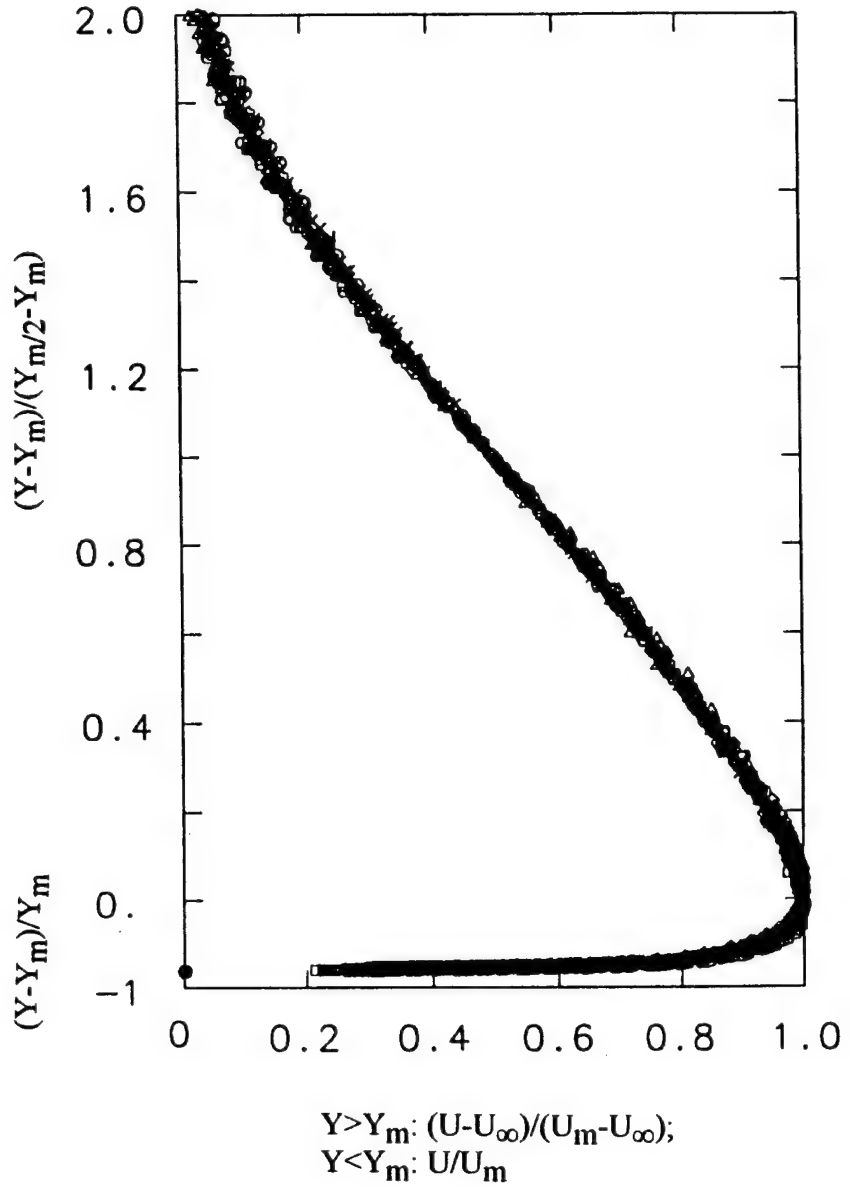

Fig.15 Mean velocity profiles in the downstream region of the first type weak wall jets normalized by two velocity scales and two length scales.

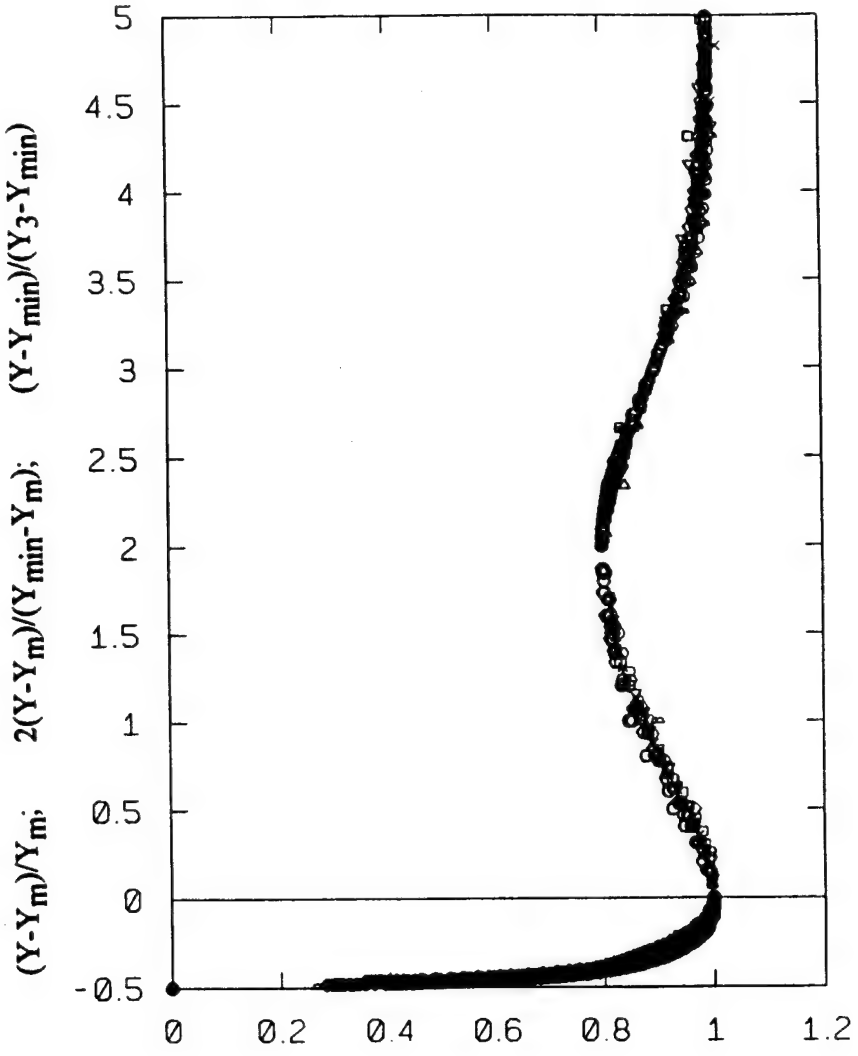

Fig.16 Mean velocity profiles in the upstream region of the second type weak wall jets normalized by three velocity scales and three length scales.

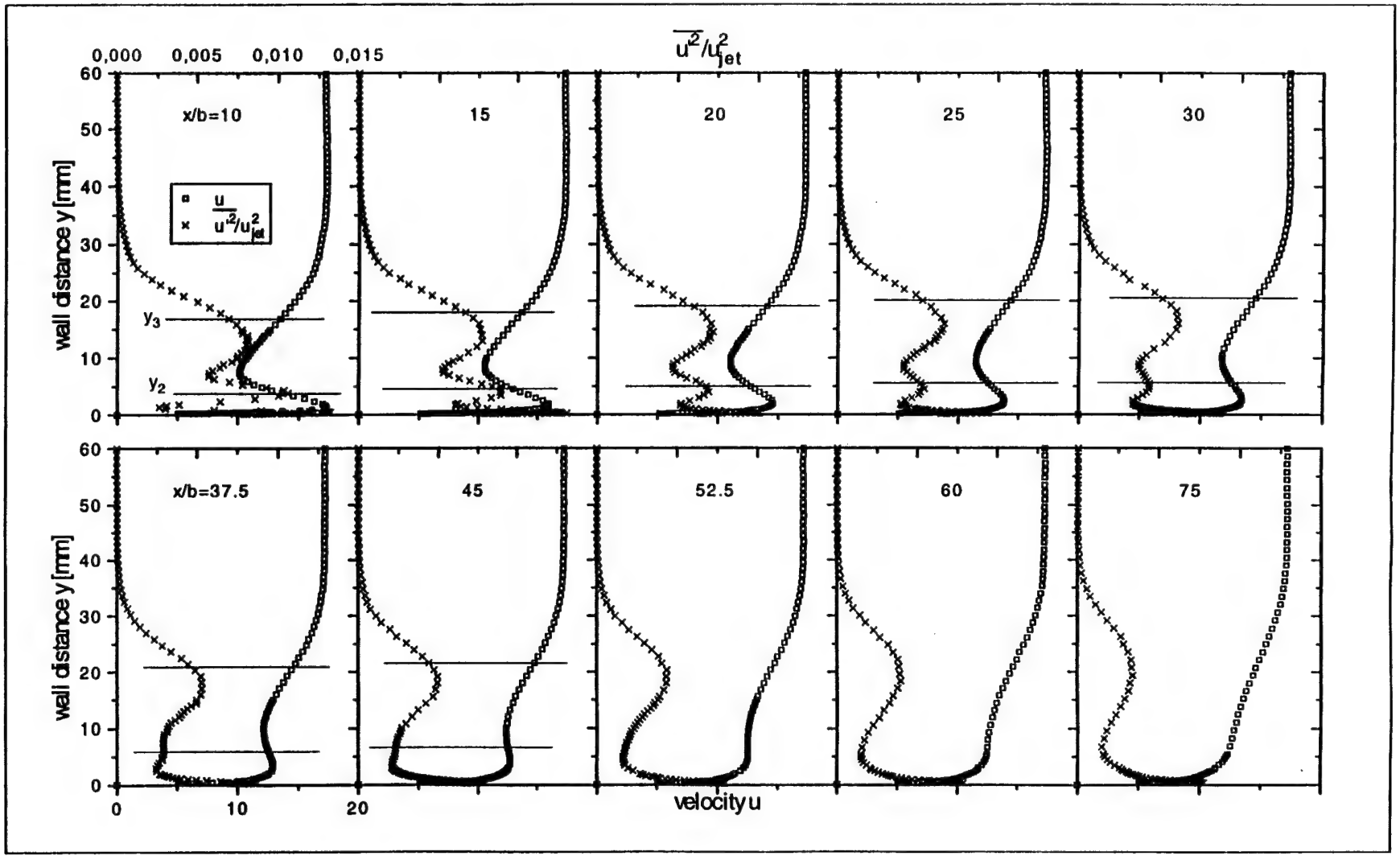

Fig.17 Turbulence energy distribution of the second type weak wall jet.

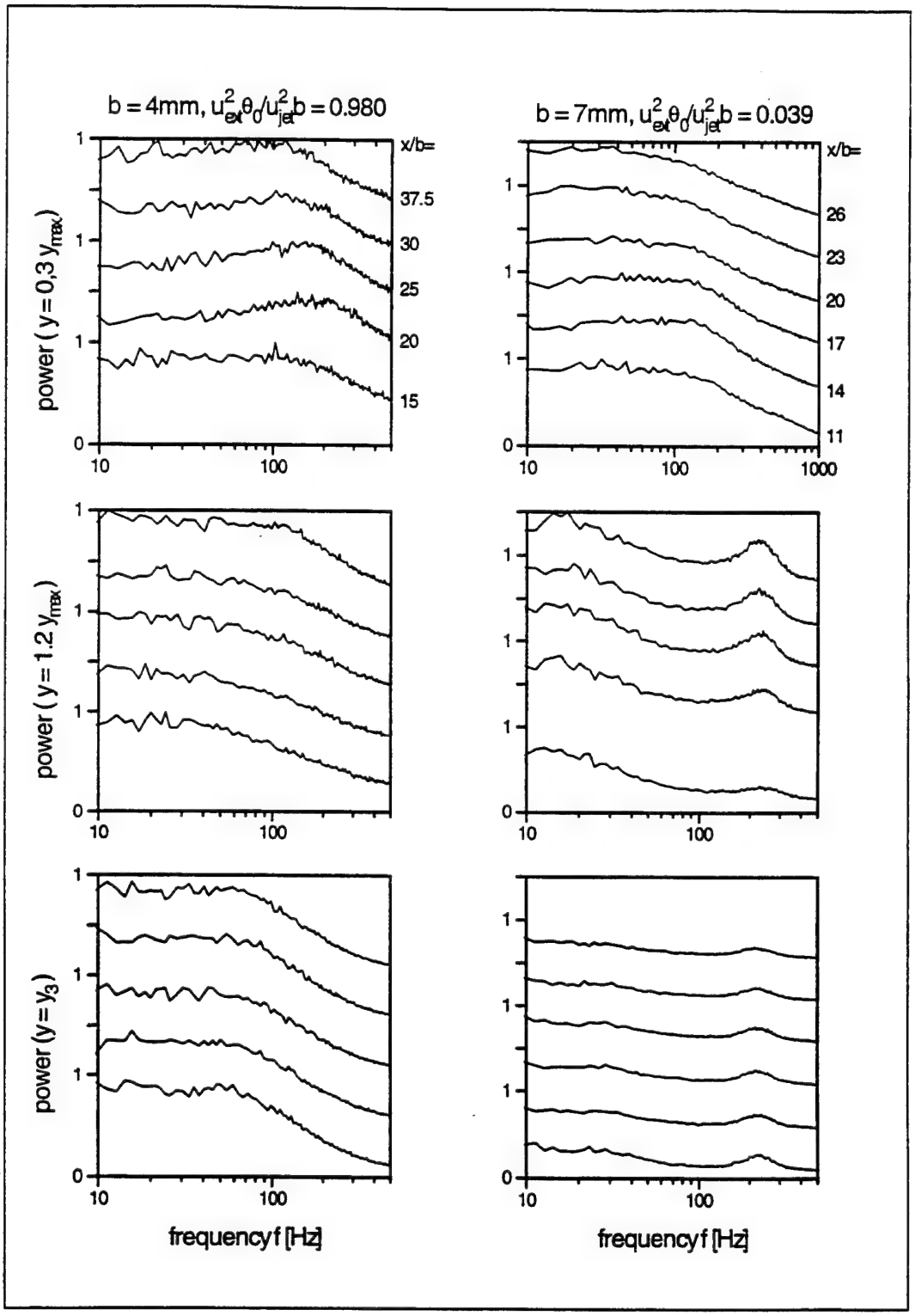

Fig.18 Power spectra in three different region of the second type weak wall jet.

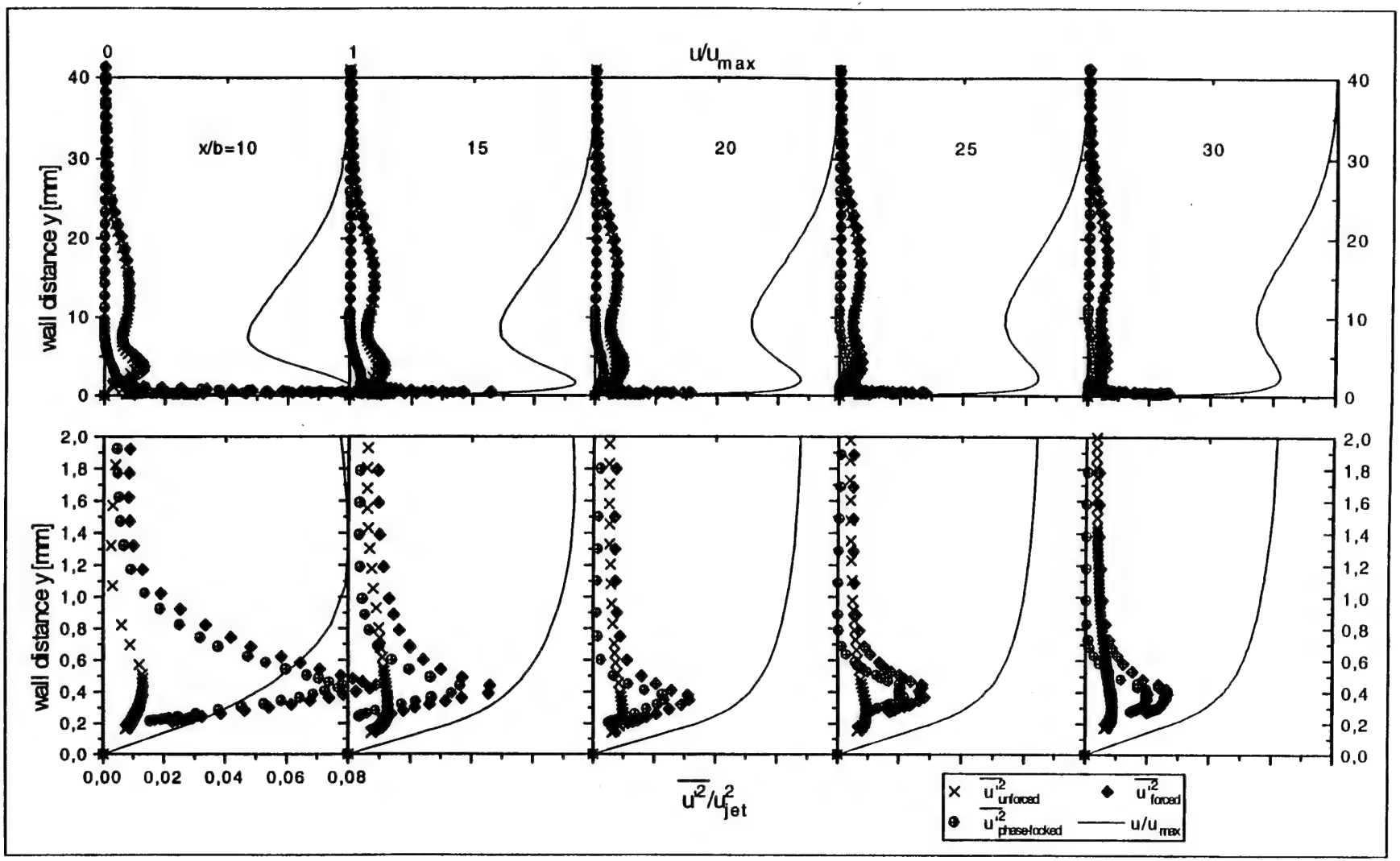

Fig.19 The total and phase-locked amplitude distribution of disturbances in the second type weak wall jet forced at a frequency corresponding to the viscous mode.

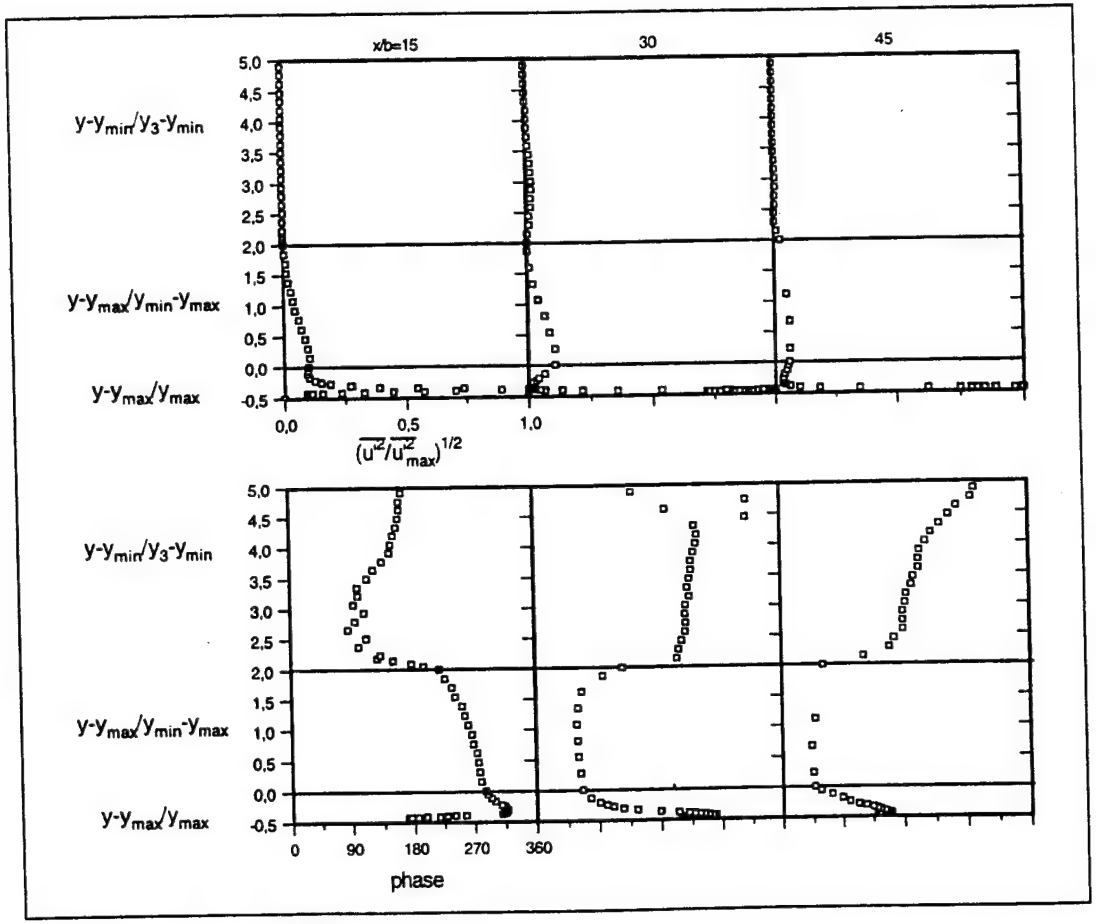

Fig.20 The phase distribution of disturbances in the second type weak wall jet forced at a frequency corresponding to the viscous mode.

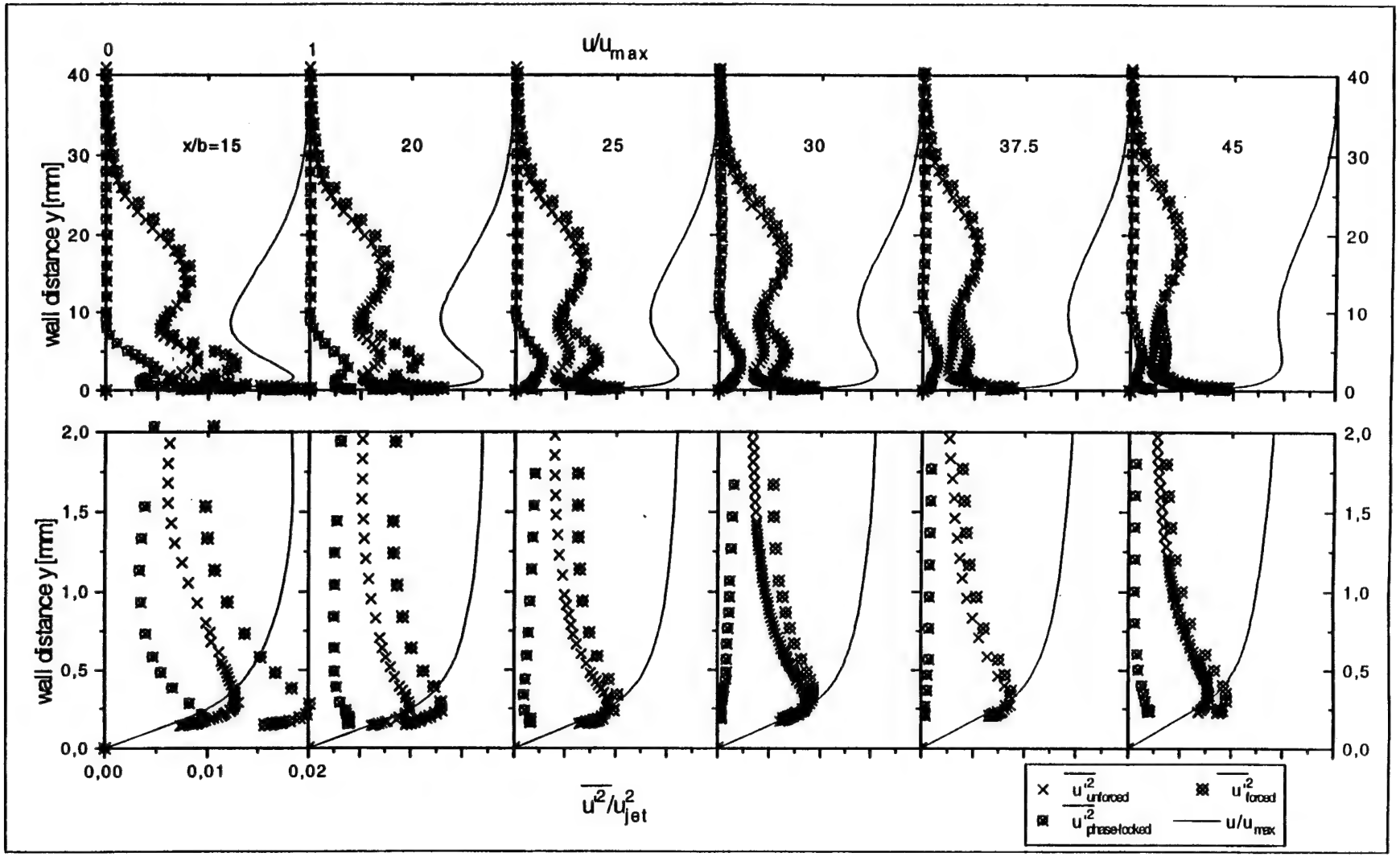

Fig.21 The total and phase-locked amplitude distribution of disturbances in the second type weak wall jet forced at a frequency corresponding to the invicid mode.

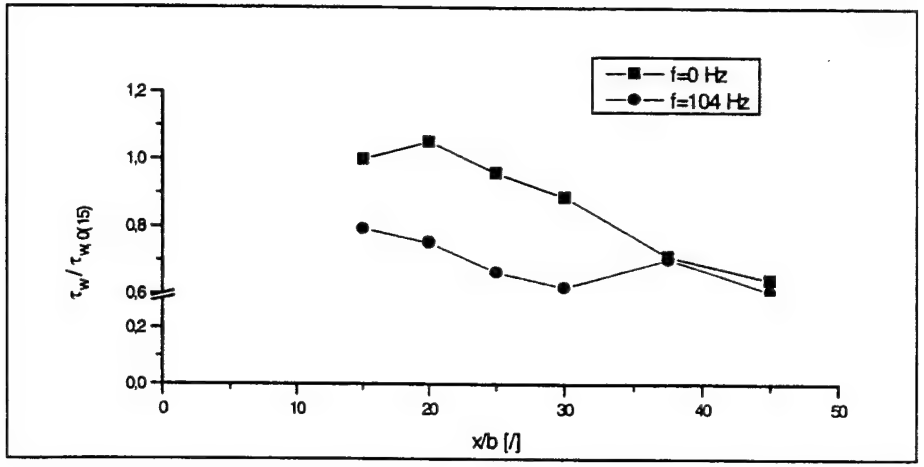

Fig.22 The skin friction reduction in the second type weak wall jet forced at a frequency corresponding to the viscous mode.

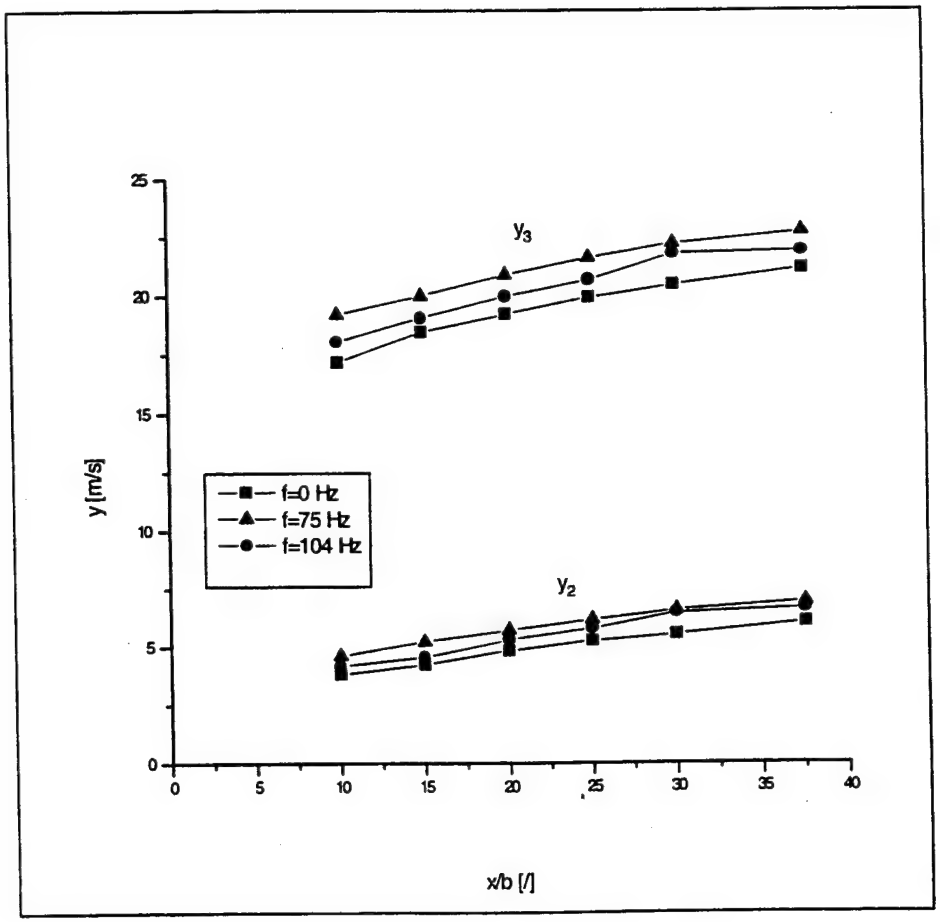

Fig.23 Comparison of the streamwise distribution of the wall jet thickness between forced and unforced flows.

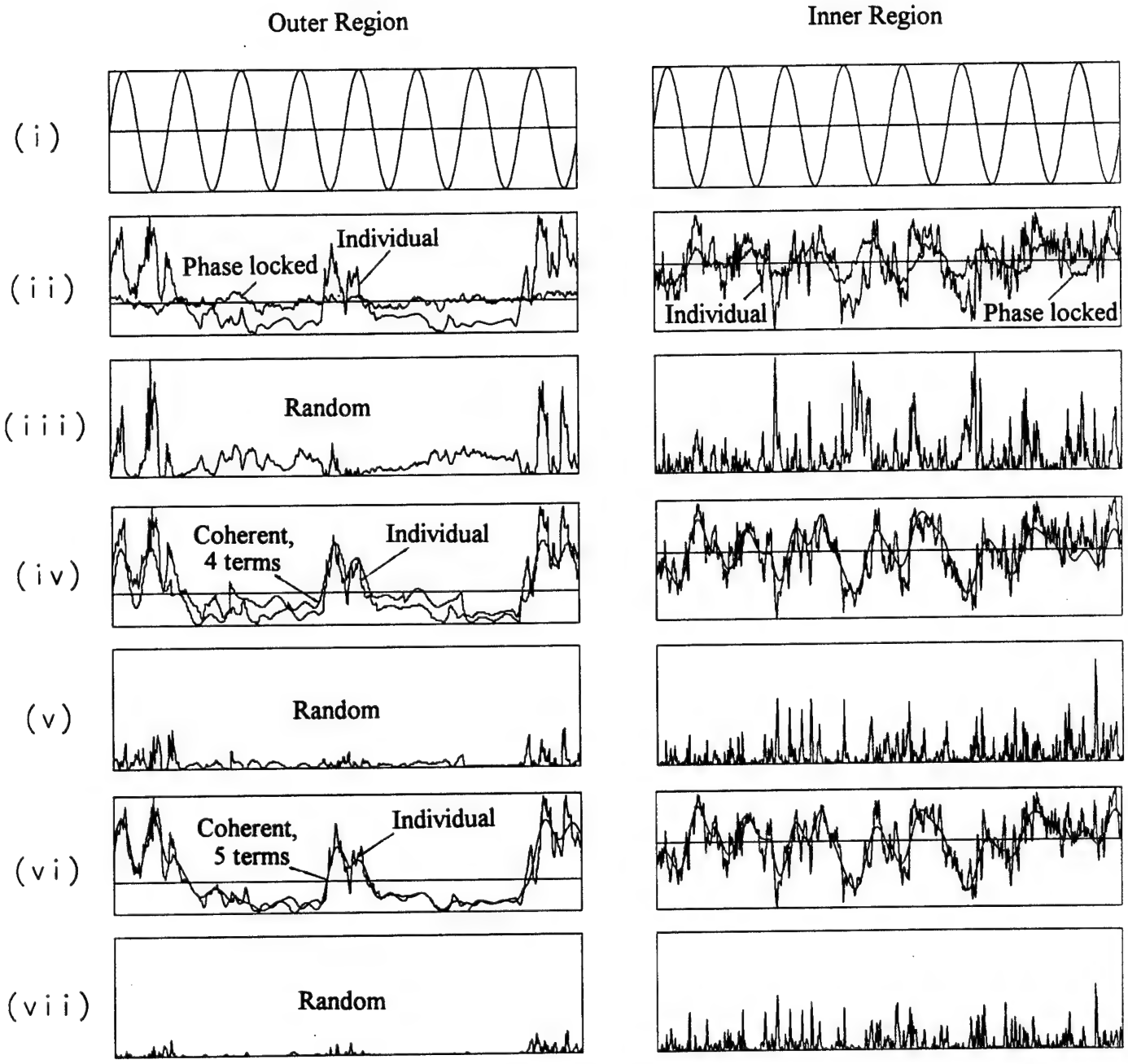

Fig.24 Reconstruction of the velocity signals by the new triple decomposition technique compared with the conventional phase-locked ensemble averaging technique.

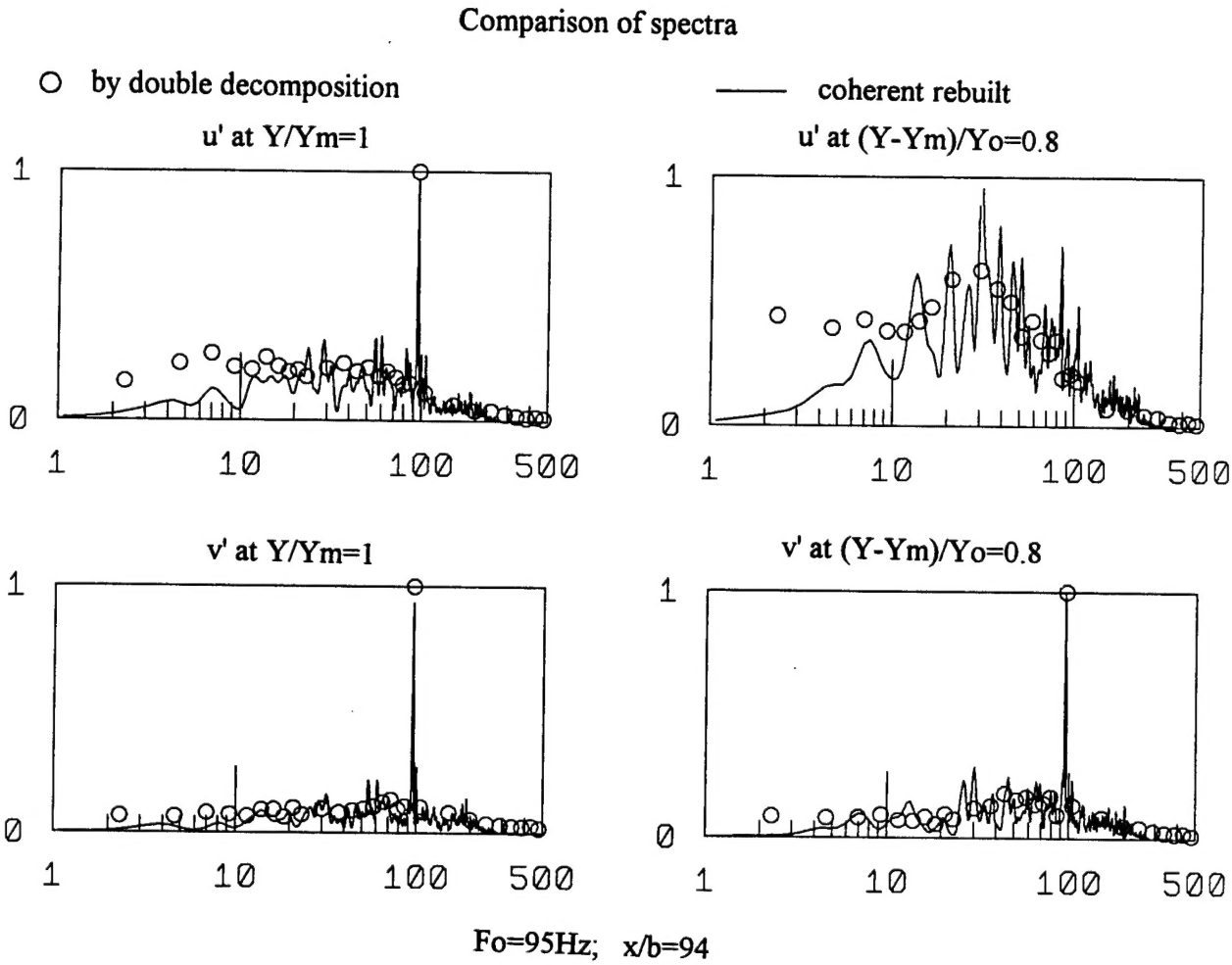

Fig.25 Reconstruction of the spectra representing the coherent motion compared with the ones representing the total fluctuations.

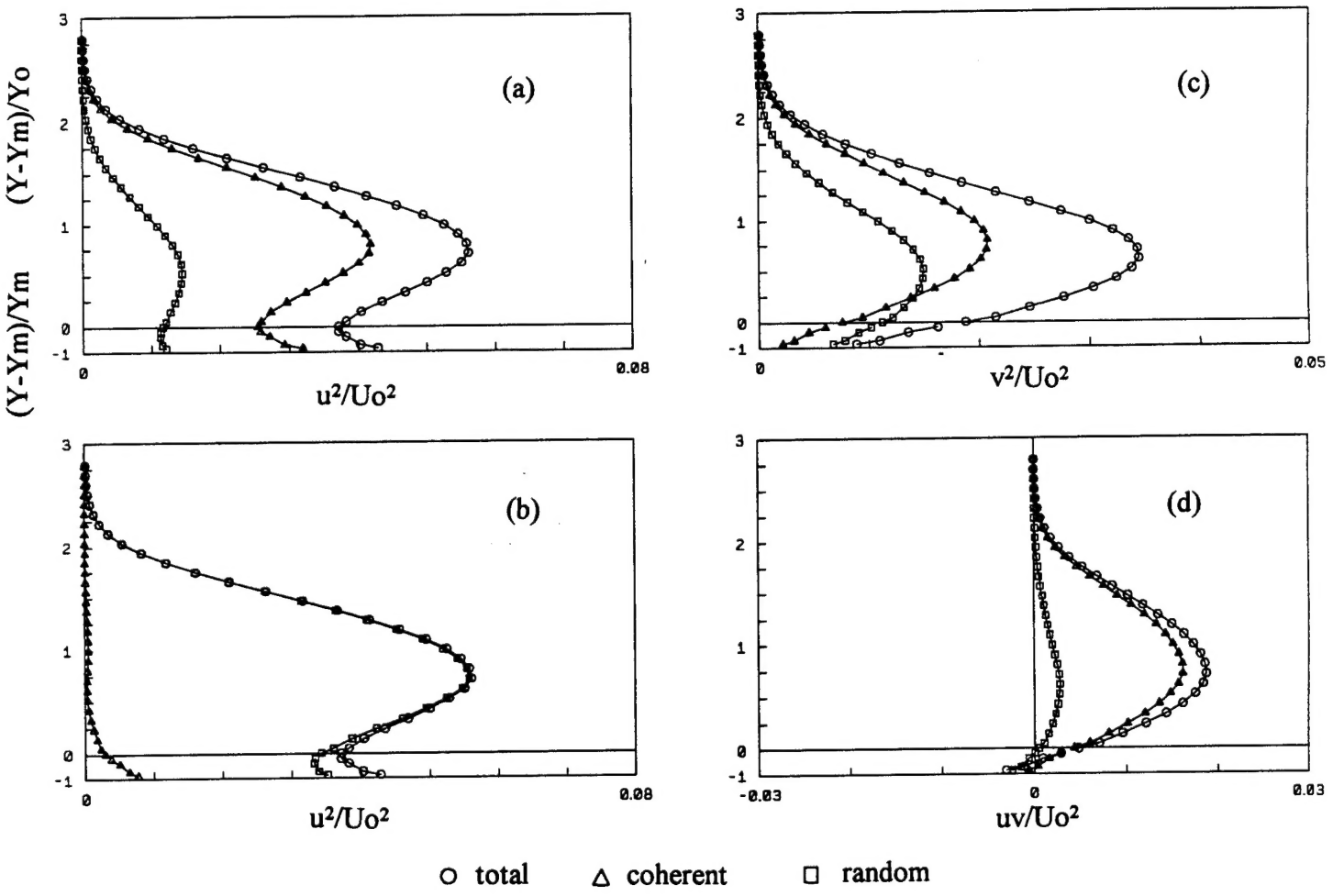

Fig.26 The comparison between the new procedure and the conventional phase-locked averaged data.
(a) streamwise component of turbulence intensity - new procedure.
(b) streamwise component of turbulence intensity - conventional procedure.
(c) normal component of turbulence intensity - new procedure.
(d) Reynolds stress - new procedure.

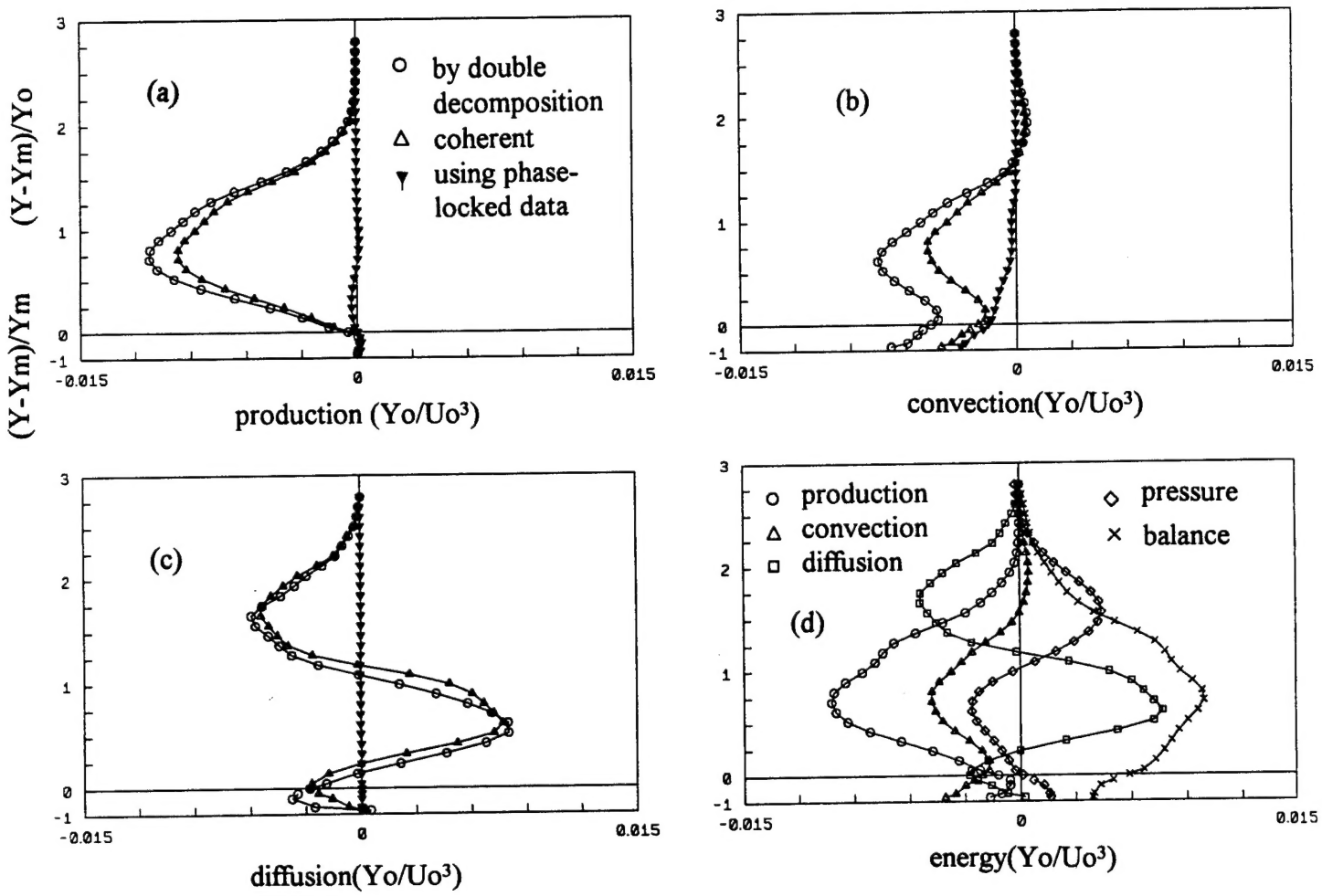

Fig.27 The kinetic energy budget for the large coherent eddies.
(a) production.
(b) convection.
(c) diffusion.
(d) energy balance.

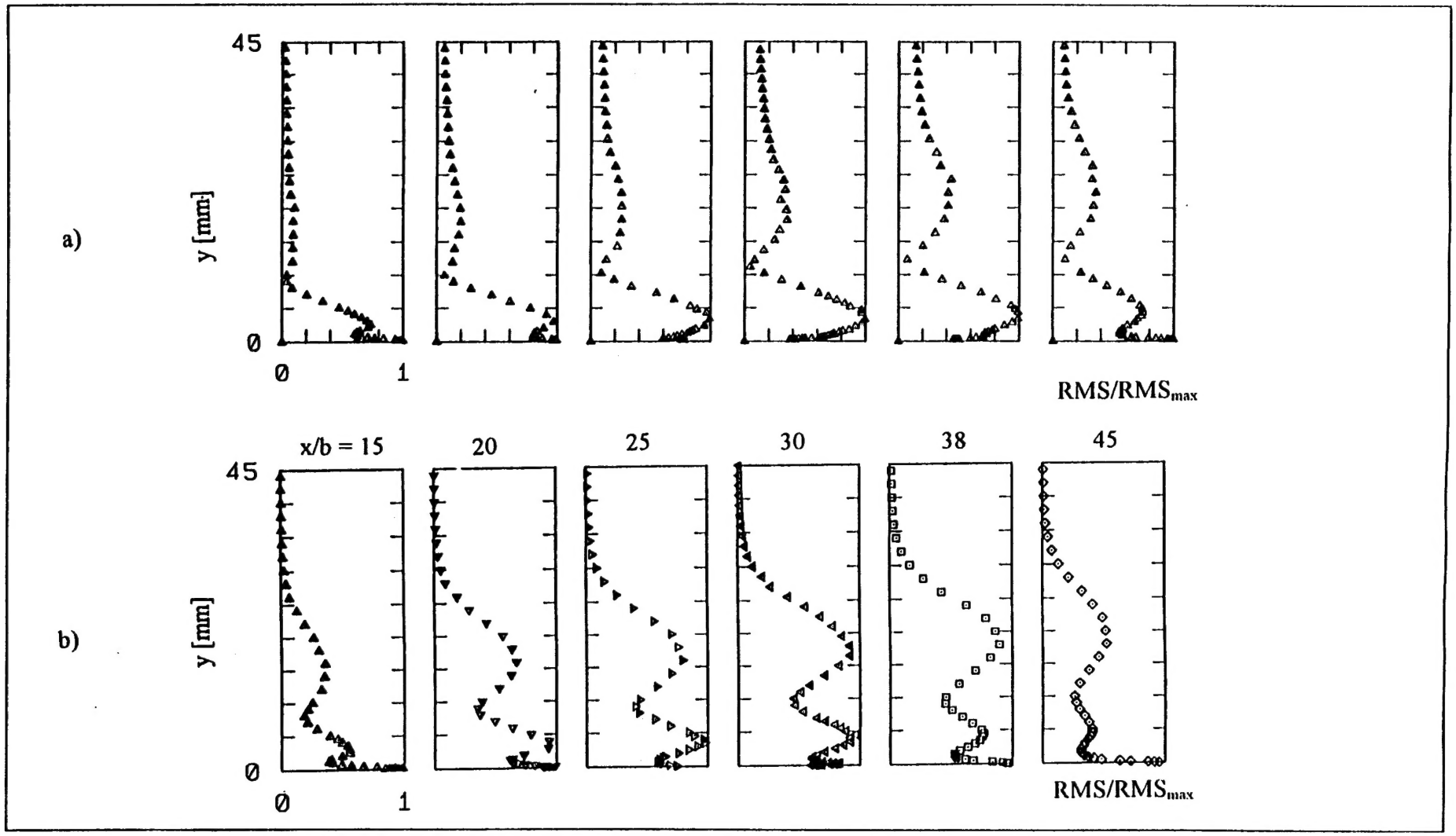

Fig.28 The normalized amplitude distribution of disturbances in the second type weak wall jet forced at a frequency corresponding to the invicid mode.
a. Calculaed by the conventional phase-locked ensemble averaging procedure.